EUROPEAN LABORATORY FOR PARTICLE PHYSICS

CERN-PPE/97-132
6th October 1997

Search for Anomalous Production of Photonic Events with Missing Energy in e^+e^- Collisions at $\sqrt{s} = 130 - 172$ GeV

The OPAL Collaboration

Abstract

Photonic events with large missing energy have been observed in e^+e^- collisions at centre-of-mass energies of 130, 136, 161 and 172 GeV using the OPAL detector at LEP. Results are presented based on search topologies designed to select events with a single photon and missing transverse energy or events with a pair of acoplanar photons. In both search topologies, cross-section measurements are performed within the kinematic acceptance of the selection. These results are compared with the expectations from the Standard Model processes $e^+e^- \to \nu\overline{\nu}\gamma(\gamma)$ (single-photon) and $e^+e^- \to \nu\overline{\nu}\gamma\gamma(\gamma)$ (acoplanar-photons). No evidence is observed for new physics contributions to these final states. Upper limits on $\sigma(e^+e^- \to XY)\cdot BR(X \to Y\gamma)$ and $\sigma(e^+e^- \to XX)\cdot BR^2(X \to Y\gamma)$ are derived for the case of stable and invisible Y. These limits apply to single and pair production of excited neutrinos ($X = \nu^*, Y = \nu$), to neutralino production ($X = \tilde{\chi}^0_2, Y = \tilde{\chi}^0_1$), and to supersymmetric models in which $X = \tilde{\chi}^0_1$ and $Y = \tilde{G}$ is a light gravitino. For the latter scenario, the results of the acoplanar-photons search are used to provide model-dependent lower limits on the mass of the lightest neutralino.

(To be submitted to Z. Phys. C)

The OPAL Collaboration

K. Ackerstaff[8], G. Alexander[23], J. Allison[16], N. Altekamp[5], K.J. Anderson[9], S. Anderson[12], S. Arcelli[2], S. Asai[24], S.F. Ashby[1], D. Axen[29], G. Azuelos[18,a], A.H. Ball[17], E. Barberio[8], R.J. Barlow[16], R. Bartoldus[3], J.R. Batley[5], S. Baumann[3], J. Bechtluft[14], C. Beeston[16], T. Behnke[8], A.N. Bell[1], K.W. Bell[20], G. Bella[23], S. Bentvelsen[8], S. Bethke[14], S. Betts[15], O. Biebel[14], A. Biguzzi[5], S.D. Bird[16], V. Blobel[27], I.J. Bloodworth[1], J.E. Bloomer[1], M. Bobinski[10], P. Bock[11], D. Bonacorsi[2], M. Boutemeur[34], S. Braibant[8], L. Brigliadori[2], R.M. Brown[20], H.J. Burckhart[8], C. Burgard[8], R. Bürgin[10], P. Capiluppi[2], R.K. Carnegie[6], A.A. Carter[13], J.R. Carter[5], C.Y. Chang[17], D.G. Charlton[1,b], D. Chrisman[4], P.E.L. Clarke[15], I. Cohen[23], J.E. Conboy[15], O.C. Cooke[8], C. Couyoumtzelis[13], R.L. Coxe[9], M. Cuffiani[2], S. Dado[22], C. Dallapiccola[17], G.M. Dallavalle[2], R. Davis[30], S. De Jong[12], L.A. del Pozo[4], K. Desch[3], B. Dienes[33,d], M.S. Dixit[7], M. Doucet[18], E. Duchovni[26], G. Duckeck[34], I.P. Duerdoth[16], D. Eatough[16], J.E.G. Edwards[16], P.G. Estabrooks[6], H.G. Evans[9], M. Evans[13], F. Fabbri[2], A. Fanfani[2], M. Fanti[2], A.A. Faust[30], L. Feld[8], F. Fiedler[27], M. Fierro[2], H.M. Fischer[3], I. Fleck[8], R. Folman[26], D.G. Fong[17], M. Foucher[17], A. Fürtjes[8], D.I. Futyan[16], P. Gagnon[7], J.W. Gary[4], J. Gascon[18], S.M. Gascon-Shotkin[17], N.I. Geddes[20], C. Geich-Gimbel[3], T. Geralis[20], G. Giacomelli[2], P. Giacomelli[4], R. Giacomelli[2], V. Gibson[5], W.R. Gibson[13], D.M. Gingrich[30,a], D. Glenzinski[9], J. Goldberg[22], M.J. Goodrick[5], W. Gorn[4], C. Grandi[2], E. Gross[26], J. Grunhaus[23], M. Gruwé[8], C. Hajdu[32], G.G. Hanson[12], M. Hansroul[8], M. Hapke[13], C.K. Hargrove[7], P.A. Hart[9], C. Hartmann[3], M. Hauschild[8], C.M. Hawkes[5], R. Hawkings[27], R.J. Hemingway[6], M. Herndon[17], G. Herten[10], R.D. Heuer[8], M.D. Hildreth[8], J.C. Hill[5], S.J. Hillier[1], P.R. Hobson[25], A. Hocker[9], R.J. Homer[1], A.K. Honma[28,a], D. Horváth[32,c], K.R. Hossain[30], R. Howard[29], P. Hüntemeyer[27], D.E. Hutchcroft[5], P. Igo-Kemenes[11], D.C. Imrie[25], M.R. Ingram[16], K. Ishii[24], A. Jawahery[17], P.W. Jeffreys[20], H. Jeremie[18], M. Jimack[1], A. Joly[18], C.R. Jones[5], G. Jones[16], M. Jones[6], U. Jost[11], P. Jovanovic[1], T.R. Junk[8], J. Kanzaki[24], D. Karlen[6], V. Kartvelishvili[16], K. Kawagoe[24], T. Kawamoto[24], P.I. Kayal[30], R.K. Keeler[28], R.G. Kellogg[17], B.W. Kennedy[20], J. Kirk[29], A. Klier[26], S. Kluth[8], T. Kobayashi[24], M. Kobel[10], D.S. Koetke[6], T.P. Kokott[3], M. Kolrep[10], S. Komamiya[24], T. Kress[11], P. Krieger[6], J. von Krogh[11], P. Kyberd[13], G.D. Lafferty[16], R. Lahmann[17], W.P. Lai[19], D. Lanske[14], J. Lauber[15], S.R. Lautenschlager[31], J.G. Layter[4], D. Lazic[22], A.M. Lee[31], E. Lefebvre[18], D. Lellouch[26], J. Letts[12], L. Levinson[26], S.L. Lloyd[13], F.K. Loebinger[16], G.D. Long[28], M.J. Losty[7], J. Ludwig[10], D. Lui[12], A. Macchiolo[2], A. Macpherson[30], M. Mannelli[8], S. Marcellini[2], C. Markopoulos[13], C. Markus[3], A.J. Martin[13], J.P. Martin[18], G. Martinez[17], T. Mashimo[24], P. Mättig[3], W.J. McDonald[30], J. McKenna[29], E.A. Mckigney[15], T.J. McMahon[1], R.A. McPherson[8], F. Meijers[8], S. Menke[3], F.S. Merritt[9], H. Mes[7], J. Meyer[27], A. Michelini[2], G. Mikenberg[26], D.J. Miller[15], A. Mincer[22,e], R. Mir[26], W. Mohr[10], A. Montanari[2], T. Mori[24], U. Müller[3], S. Mihara[24], K. Nagai[26], I. Nakamura[24], H.A. Neal[8], B. Nellen[3], R. Nisius[8], S.W. O'Neale[1], F.G. Oakham[7], F. Odorici[2], H.O. Ogren[12], A. Oh[27], N.J. Oldershaw[16], M.J. Oreglia[9], S. Orito[24], J. Pálinkás[33,d], G. Pásztor[32], J.R. Pater[16], G.N. Patrick[20], J. Patt[10], R. Perez-Ochoa[8], S. Petzold[27], P. Pfeifenschneider[14], J.E. Pilcher[9], J. Pinfold[30], D.E. Plane[8], P. Poffenberger[28], B. Poli[2], A. Posthaus[3], C. Rembser[8], S. Robertson[28], S.A. Robins[22], N. Rodning[30], J.M. Roney[28], A. Rooke[15], A.M. Rossi[2], P. Routenburg[30], Y. Rozen[22], K. Runge[10], O. Runolfsson[8], U. Ruppel[14], D.R. Rust[12], R. Rylko[25], K. Sachs[10], T. Saeki[24], W.M. Sang[25], E.K.G. Sarkisyan[23], C. Sbarra[29], A.D. Schaile[34], O. Schaile[34], F. Scharf[3], P. Scharff-Hansen[8], J. Schieck[11], P. Schleper[11], B. Schmitt[8], S. Schmitt[11], A. Schöning[8], M. Schröder[8], H.C. Schultz-Coulon[10], M. Schumacher[3], C. Schwick[8], W.G. Scott[20], T.G. Shears[16], B.C. Shen[4], C.H. Shepherd-Themistocleous[8], P. Sherwood[15], G.P. Siroli[2], A. Sittler[27], A. Skillman[15], A. Skuja[17], A.M. Smith[8], G.A. Snow[17], R. Sobie[28], S. Söldner-Rembold[10], R.W. Springer[30], M. Sproston[20], K. Stephens[16], J. Steuerer[27], B. Stockhausen[3], K. Stoll[10], D. Strom[19], R. Ströhmer[34], P. Szymanski[20], R. Tafirout[18], S.D. Talbot[1], S. Tanaka[24], P. Taras[18], S. Tarem[22], R. Teuscher[8], M. Thiergen[10], M.A. Thomson[8], E. von Törne[3], E. Torrence[8], S. Towers[6], I. Trigger[18], Z. Trócsányi[33], E. Tsur[23], A.S. Turcot[9], M.F. Turner-Watson[8],

P. Utzat[11], R. Van Kooten[12], M. Verzocchi[10], P. Vikas[18], E.H. Vokurka[16], H. Voss[3], F. Wäckerle[10], A. Wagner[27], C.P. Ward[5], D.R. Ward[5], P.M. Watkins[1], A.T. Watson[1], N.K. Watson[1], P.S. Wells[8], N. Wermes[3], J.S. White[28], B. Wilkens[10], G.W. Wilson[27], J.A. Wilson[1], T.R. Wyatt[16], S. Yamashita[24], G. Yekutieli[26], V. Zacek[18], D. Zer-Zion[8]

[1]School of Physics and Space Research, University of Birmingham, Birmingham B15 2TT, UK
[2]Dipartimento di Fisica dell' Università di Bologna and INFN, I-40126 Bologna, Italy
[3]Physikalisches Institut, Universität Bonn, D-53115 Bonn, Germany
[4]Department of Physics, University of California, Riverside CA 92521, USA
[5]Cavendish Laboratory, Cambridge CB3 0HE, UK
[6] Ottawa-Carleton Institute for Physics, Department of Physics, Carleton University, Ottawa, Ontario K1S 5B6, Canada
[7]Centre for Research in Particle Physics, Carleton University, Ottawa, Ontario K1S 5B6, Canada
[8]CERN, European Organisation for Particle Physics, CH-1211 Geneva 23, Switzerland
[9]Enrico Fermi Institute and Department of Physics, University of Chicago, Chicago IL 60637, USA
[10]Fakultät für Physik, Albert Ludwigs Universität, D-79104 Freiburg, Germany
[11]Physikalisches Institut, Universität Heidelberg, D-69120 Heidelberg, Germany
[12]Indiana University, Department of Physics, Swain Hall West 117, Bloomington IN 47405, USA
[13]Queen Mary and Westfield College, University of London, London E1 4NS, UK
[14]Technische Hochschule Aachen, III Physikalisches Institut, Sommerfeldstrasse 26-28, D-52056 Aachen, Germany
[15]University College London, London WC1E 6BT, UK
[16]Department of Physics, Schuster Laboratory, The University, Manchester M13 9PL, UK
[17]Department of Physics, University of Maryland, College Park, MD 20742, USA
[18]Laboratoire de Physique Nucléaire, Université de Montréal, Montréal, Quebec H3C 3J7, Canada
[19]University of Oregon, Department of Physics, Eugene OR 97403, USA
[20]Rutherford Appleton Laboratory, Chilton, Didcot, Oxfordshire OX11 0QX, UK
[22]Department of Physics, Technion-Israel Institute of Technology, Haifa 32000, Israel
[23]Department of Physics and Astronomy, Tel Aviv University, Tel Aviv 69978, Israel
[24]International Centre for Elementary Particle Physics and Department of Physics, University of Tokyo, Tokyo 113, and Kobe University, Kobe 657, Japan
[25]Brunel University, Uxbridge, Middlesex UB8 3PH, UK
[26]Particle Physics Department, Weizmann Institute of Science, Rehovot 76100, Israel
[27]Universität Hamburg/DESY, II Institut für Experimental Physik, Notkestrasse 85, D-22607 Hamburg, Germany
[28]University of Victoria, Department of Physics, P O Box 3055, Victoria BC V8W 3P6, Canada
[29]University of British Columbia, Department of Physics, Vancouver BC V6T 1Z1, Canada
[30]University of Alberta, Department of Physics, Edmonton AB T6G 2J1, Canada
[31]Duke University, Dept of Physics, Durham, NC 27708-0305, USA
[32]Research Institute for Particle and Nuclear Physics, H-1525 Budapest, P O Box 49, Hungary
[33]Institute of Nuclear Research, H-4001 Debrecen, P O Box 51, Hungary
[34]Ludwigs-Maximilians-Universität München, Sektion Physik, Am Coulombwall 1, D-85748 Garching, Germany

[a] and at TRIUMF, Vancouver, Canada V6T 2A3
[b] and Royal Society University Research Fellow
[c] and Institute of Nuclear Research, Debrecen, Hungary
[d] and Department of Experimental Physics, Lajos Kossuth University, Debrecen, Hungary
[e] and Department of Physics, New York University, NY 1003, USA

1 Introduction

This paper describes a search for photonic events with large missing energy in e^+e^- collisions at centre-of-mass energies of 130, 136, 161 and 172 GeV. Two different search topologies are used. Cross-section measurements and search results from single-photon and acoplanar-photons topologies at $\sqrt{s} = 130$-136 GeV [1] and $\sqrt{s} = 161$ GeV [2] have been previously published. Those results have also been used to search for excited neutrinos with photonic decays at $\sqrt{s} = 130$-136 GeV [3] and $\sqrt{s} = 161$ GeV [4]. In the analyses presented in this paper, both the single and acoplanar-photons search techniques are based on those previously published by OPAL, but in each case the kinematic acceptance of the analysis has been extended to lower energy and more forward angles, and the efficiency has been increased by allowing for the possibility of photon conversions. These results supersede our previous results.

The single-photon and acoplanar-photons search topologies presented here are designed to select events with one or more photons and significant missing transverse energy, indicating the presence of at least one neutrino-like invisible particle which interacts only weakly with matter. Results on photonic events without missing energy are presented in a separate paper. [5].

The single-photon search topology is sensitive to neutral events in which there are one or two photons and missing energy, which within the Standard Model are expected from the $e^+e^- \to \nu\overline{\nu}\gamma(\gamma)$ process. Measurements of single-photon production have been made in e^+e^- collisions at the Z^0 and at lower energies [6–8]. Results from centre-of-mass energies significantly above the Z^0 mass have also been reported [1, 9]. The expected visible energies are sufficiently large at present centre-of-mass energies that doubly radiative neutrino pair production can lead to two photons being detected; the experimental topology therefore includes such cases.

The acoplanar-photons search topology is designed to select neutral events with two or more photons and significant missing transverse energy, which within the Standard Model are expected from the $e^+e^- \to \nu\overline{\nu}\gamma\gamma(\gamma)$ process. The selection is designed to retain acceptance for events with a number of photons, N_γ, greater than two if the system formed by the three most energetic photons shows evidence for significant missing transverse energy.

These photonic final-state topologies are sensitive to new physics of the type $e^+e^- \to XY$ and $e^+e^- \to XX$ where X is neutral and decays radiatively ($X \to Y\gamma$) and Y is stable and only weakly interacting. For the general case of massive X and Y this includes conventional supersymmetric processes [10] ($X = \tilde{\chi}^0_2, Y = \tilde{\chi}^0_1$). In this context it has been emphasised [11] that the radiative branching ratio of the $\tilde{\chi}^0_2$ may be large. There is particularly good sensitivity for the special case of $M_Y \approx 0$ that applies both to the production of excited neutrinos ($X = \nu^*, Y = \nu$) and to supersymmetric models in which the lightest supersymmetric particle (LSP) is a light gravitino[1], and $\tilde{\chi}^0_1$ is the next-to-lightest supersymmetric particle (NLSP) which decays to a gravitino and a photon, ($X = \tilde{\chi}^0_1, Y = \tilde{G}$). In this case, the branching ratio of this decay of the $\tilde{\chi}^0_1$ is naturally large. Such a signature has been discussed in [12] and more recently in [13–15] for a no-scale supergravity model and in [16] for a model with gauge-mediated supersymmetry breaking; in each case, $\tilde{\chi}^0_1\tilde{\chi}^0_1$ production cross-sections of order 1 pb are predicted at these centre-of-mass energies, for $M_{\tilde{\chi}^0_1} \approx 50$ GeV. Other types of new physics to which these search topologies are sensitive include the production of invisible particles made visible through initial-state radiation and the production of an invisible particle in association with a photon. The acoplanar-photons search topology also has sensitivity to the production of two particles, one invisible, or with an invisible decay mode, and the other decaying into two photons. Such events might arise from the production of a Higgs-like particle, $S^0 : e^+e^- \to Z^0S^0$, followed by $S^0 \to \gamma\gamma$, $Z^0 \to \nu\overline{\nu}$. Results

[1] The mass scale is typically $\mathcal{O}$(keV).

for this model searching for the hadronic and leptonic Z^0 decays appear elsewhere [17].

This paper will first briefly describe the detector, the data sample and the Monte Carlo samples used, including a discussion of event generators for $e^+e^- \to \nu\overline{\nu} + n\gamma$. The event selection for each search topology will then be described, followed by cross-section measurements for $e^+e^- \to \nu\overline{\nu}\gamma(\gamma)$ and $e^+e^- \to \nu\overline{\nu}\gamma\gamma(\gamma)$ and comparisons with Standard Model expectations. Implications of these results on the possibility of new physics processes of the type $e^+e^- \to XY$ or XX, $X \to Y\gamma$ will be discussed.

2 Detector, Data Sample and Monte Carlo Samples

The OPAL detector is described in detail elsewhere [18]. The measurements presented here are mainly based on the observation of clusters of energy deposited in the lead-glass electromagnetic calorimeters (ECAL) consisting of a 9,440 lead glass block array in the barrel ($|\cos\theta| < 0.82$) with a quasi-pointing geometry, and two dome-shaped endcap arrays, each of 1,132 lead-glass blocks with axes coaxial with the beam axis covering the polar angle range ($0.81 < |\cos\theta| < 0.984$). In the overlap region, $0.785 < |\cos\theta| < 0.815$, and at very forward angles, $|\cos\theta| > 0.94$ the energy-resolution of the ECAL is slightly degraded relative to the nominal resolution. In some cases (where stated) these regions have been excluded from the analysis. These calorimeters, together with the gamma-catcher calorimeter, the forward calorimeters and the silicon-tungsten calorimeter (SiW), provide a fully hermetic electromagnetic calorimeter down to polar angles of 33 mrad. The SiW calorimeter covers polar angles down to 24 mrad, however the region around 30 mrad lacks useful calorimetric coverage due to the installation, in 1996, of a thick tungsten shield designed to protect the tracking chambers from accelerator backgrounds while running at centre-of-mass energies well above the Z^0 resonance. The tracking system, consisting of a silicon microvertex detector, a vertex drift chamber (CV) and a large volume jet drift chamber (CJ), is used to reject events with prompt charged particles. The silicon microvertex detector consists of two concentric cylindrical layers of silicon microstrip arrays, each layer providing both an azimuthal and longitudinal (along the beam direction) coordinate measurement. The two layer acceptance covers $|\cos\theta| < 0.90$ for the 161 and 172 GeV data-set while for the data acquired in 1995 at 130 and 136 GeV, the acceptance is limited to $|\cos\theta| < 0.75$. Beam-related backgrounds and backgrounds arising from cosmic-ray interactions are rejected using information from the time-of-flight system, (TOF), the hadron calorimeter and muon detectors.

The data used in this analysis were recorded at e^+e^- centre-of-mass energies of 130.3, 136.2, 161.3, and 172.1 GeV, with integrated luminosities of 2.30, 2.59, 9.89, and 10.28 pb^{-1}, respectively. The integrated luminosities are determined to better than 1% from small-angle Bhabha scattering events in the SiW luminosity calorimeter. Triggers [19] based on electromagnetic energy deposits in either the barrel or endcap electromagnetic calorimeters, and also on a coincidence of energy in the barrel electromagnetic calorimeter and a hit in the TOF system, lead to full trigger efficiency for photonic events passing the event selection criteria described below.

For the expected Standard Model signal process, $e^+e^- \to \nu\overline{\nu} + n\gamma$, the Monte Carlo generators NNGG03 [20], NUNUGPV [21] and KORALZ [22] were used. Modelling of these backgrounds is discussed in more detail in section 2.1. For other expected Standard Model background processes, a number of different generators were used: RADCOR [23] for $e^+e^- \to \gamma\gamma(\gamma)$; BHWIDE [24] and TEEGG [25] for $e^+e^- \to e^+e^-(\gamma)$; and KORALZ for $e^+e^- \to \mu^+\mu^-(\gamma)$ and $e^+e^- \to \tau^+\tau^-(\gamma)$.

To simulate possible new physics processes of the type $e^+e^- \to XY$ and $e^+e^- \to XX$ where X decays to $Y\gamma$ and Y escapes detection, the SUSYGEN [26] Monte Carlo generator was used to produce neutralino pair events of the type $e^+e^- \to \tilde{\chi}_2^0\tilde{\chi}_1^0$ and $e^+e^- \to \tilde{\chi}_2^0\tilde{\chi}_2^0$, $\tilde{\chi}_2^0 \to \tilde{\chi}_1^0\gamma$, with isotropic angular

distributions for the production and decay of $\tilde{\chi}_2^0$ and including initial-state radiation. SUSYGEN Monte Carlo events were generated at each centre-of-mass energy, for 16-24 points in the kinematically accessible region of the ($M_{\rm X}$, $M_{\rm Y}$) plane for which $M_{\rm X} - M_{\rm Y} \geq 5$ GeV, depending on the centre-of-mass energy. For the case $M_{\rm Y} \approx 0$, the efficiencies for XY and XX production obtained from these Monte Carlo samples are consistent within statistical errors with the efficiencies obtained from the OPAL $\nu^*\bar{\nu}$ and $\nu^*\bar{\nu}^*$ excited neutrino Monte Carlo samples respectively [3]. All the Monte Carlo samples described above were processed through the OPAL detector simulation [27].

2.1 Event Generators and Analytical Calculations of $e^+e^- \to \nu\overline{\nu} + n\gamma$

The present status of event generators for the Standard Model process $e^+e^- \to \nu\overline{\nu} + n\gamma$, $n \geq 1$, is very unsatisfactory for the centre-of-mass energy region, 130 GeV $< \sqrt{s} <$ 172 GeV, relevant to the analyses presented here.

For $\sqrt{s} \approx M_{\rm Z}$, two event generators, NNGG03 and KORALZ were used extensively for studies of $e^+e^- \to \nu\overline{\nu}\gamma(\gamma)$ with a demonstrated agreement [28] between the cross-section predictions of better than 1%. NNGG03 is designed for $e^+e^- \to \nu\overline{\nu}\gamma(\gamma)$ at $\sqrt{s} \approx M_{\rm Z}$ with inclusive exponentiation of soft photons and the hard photon matrix element for $e^+e^- \to \nu\overline{\nu}\gamma\gamma(\gamma)$ for the Z exchange diagrams only. At higher centre-of-mass energies, it has not been maintained officially by the authors, nor claimed to be reliable. The absence of a complete lowest order calculation for $e^+e^- \to \nu\overline{\nu}\gamma\gamma$ and higher order corrections ($e^+e^- \to \nu\overline{\nu}\gamma\gamma(\gamma)$) make it necessarily incomplete for $e^+e^- \to \nu\overline{\nu}\gamma\gamma(\gamma)$. The KORALZ event generator, primarily designed for $e^+e^- \to \mu^+\mu^-(\gamma)$ and $e^+e^- \to \tau^+\tau^-(\gamma)$ at $\sqrt{s} \approx M_Z$, can also generate $e^+e^- \to \nu\overline{\nu} + n\gamma$, $n \geq 0$, using the Yennie-Frautschi-Suura approach [29] to explicitly generate an arbitrary number of additional initial state photons. This generator is maintained by the authors for $\sqrt{s} \gg M_{\rm Z}$, but no specific publications exist yet attesting to its accuracy for either $\nu\overline{\nu}\gamma(\gamma)$ or $\nu\overline{\nu}\gamma\gamma(\gamma)$ in this regime. The NUNUGPV analytical calculation is designed for $\sqrt{s} \approx M_{\rm Z}$ and $\sqrt{s} \gg M_{\rm Z}$ using the p_T dependent structure function approach to estimate $e^+e^- \to \nu\overline{\nu}\gamma(\gamma)$ with a claimed accuracy of 1-2% for 150 $< \sqrt{s} <$ 175 GeV. An event generator based on this calculation is also available which includes the emission of an additional photon from each beam. This feature is designed to permit estimation of the effect of $\nu\overline{\nu}\gamma\gamma(\gamma)$ events on the $\nu\overline{\nu}\gamma(\gamma)$ acceptance. It is not intended as an accurate estimate of the $\nu\overline{\nu}\gamma\gamma(\gamma)$ cross-section. In a previous publication [2], we used this feature inappropriately to estimate the expected contribution from $e^+e^- \to \nu\overline{\nu}\gamma\gamma(\gamma)$.

Recently, independent calculations have been made of the $e^+e^- \to \nu\overline{\nu}\gamma\gamma$ (lowest order) cross-section using CompHep [30] (by Ambrosanio [31]), and using HELAS [32] (by Mrenna [33]). Calculations of the $e^+e^- \to \nu\overline{\nu}\gamma\gamma(\gamma)$ cross-section by Mrenna, and by Bain and Pain [34] using GRACE [35] and CompHep have also been made. These are approximately a factor of two lower than the $\nu\overline{\nu}\gamma\gamma(\gamma)$ cross-section predictions we obtain using the NNGG03 and NUNUGPV event generators. The estimated $\nu\overline{\nu}\gamma\gamma(\gamma)$ cross-section from KORALZ agrees reasonably well with the independent calculations. For $e^+e^- \to \nu\overline{\nu}\gamma(\gamma)$, we have found that the estimated cross-section from KORALZ is lower by about 10% compared with NUNUGPV within the kinematic acceptance of the single-photon selection, described in section 1.

KORALZ is used to estimate the detection efficiency of $e^+e^- \to \nu\overline{\nu}\gamma(\gamma)$ and $e^+e^- \to \nu\overline{\nu}\gamma\gamma(\gamma)$ given its more complete treatment of events with multiple photons. Generator studies indicate that it also provides a reasonable estimate of the fraction of two photon events ($e^+e^- \to \nu\overline{\nu}\gamma\gamma(\gamma)$). The estimated efficiencies obtained using KORALZ are compared with those obtained using NNGG03 and NUNUGPV and only small differences are found, indicating that the experimentally measured cross-sections are relatively insensitive to the choice of generator.

For coherence in the comparisons of data with Monte Carlo, we use KORALZ. In calculating upper limits on new processes for the single-photon topology, despite the claimed 1-2% accuracy of NUNUGPV, we use the background estimate from KORALZ which is the lower of the two and is therefore expected to be conservative. Given the current status of calculations of $e^+e^- \to \nu\overline{\nu}\gamma\gamma(\gamma)$, where factor of two differences between some cross-section estimates are not yet fully understood, in calculating limits on new processes for the acoplanar-photons topology we do not take into account the $\nu\overline{\nu}\gamma\gamma(\gamma)$ background estimate.

3 Photonic Event Selection

This section describes the criteria for selecting single-photon and acoplanar-photons events. The kinematic acceptance of each topology is defined in terms of the photon energy, E_γ and the photon polar angle, θ, defined with respect to the electron beam direction. In order to simultaneously maintain sensitivity to low photon energies and to retain acceptance at high polar angles, the kinematic acceptance of each selection is composed of two (possibly overlapping) parts:

Single-Photon - One or two photons accompanied by invisible particle(s):

- At least one photon with $x_T > 0.05$ and $|\cos\theta| < 0.82$, or,
- At least one photon with $x_T > 0.1$ and $(0.82 < |\cos\theta| < 0.966)$.

Acoplanar-Photons - Two or more photons accompanied by invisible particle(s):

- At least two photons with $x_\gamma > 0.05$ and $15^\circ < \theta < 165^\circ$, or,
- One photon with $E_\gamma > 1.75$ GeV and $|\cos\theta| < 0.8$ and a second photon satisfying $E_\gamma > 1.75$ GeV and $15^\circ < \theta < 165^\circ$ ($|\cos\theta| < 0.966$).

where the scaled energy, x_γ, is defined as $E_\gamma/E_{\rm beam}$, and the scaled transverse momentum, x_T, is defined as $E_\gamma \sin\theta/E_{\rm beam}$.

In each of the topologies, it is desirable to retain acceptance for events with an additional photon, if the resulting multi-photon system is still consistent with the presence in the event of significant missing energy. This reduces the sensitivity of each measurement to the modelling of higher-order contributions.

3.1 Single-Photon Event Selection Description

Events pass the single-photon selection if they satisfy the criteria listed below. These selection criteria are similar to previous OPAL analyses of photonic events with missing energy but have increased acceptance and efficiency:

- **Angular acceptance and minimum transverse energy.** An event is considered to contain a photon candidate if the primary electromagnetic cluster (that with the highest deposited energy in the barrel or endcap calorimeters) is in the region $15^\circ < \theta < 165^\circ$ ($|\cos\theta| < 0.966$) and has a scaled transverse energy, x_T, that exceeds 0.1. Events with a primary cluster having $0.05 < x_T < 0.1$ and in the barrel region $|\cos\theta| < 0.82$ are also accepted if they have associated

TOF information with good timing, as described in the fourth selection criterion below. Events are considered to have more than one photon if additional electromagnetic clusters are found in the barrel or endcap calorimeter ($|\cos\theta| < 0.984$) having deposited energy exceeding 300 MeV.

- **Charged track veto or photon conversion consistency requirements.** Events are vetoed if there is a charged track with ten or more hits in the central detector, unless the track is consistent with arising from a photon conversion. Events having no charged tracks are called non-conversion candidates. Photon conversion consistency requires that the primary photon candidate cluster be associated with the highest p_T track in the event within 100 mrad in both azimuthal and polar angle. This track should not be prompt, i.e. the cluster is not accepted as a possible photon conversion if there are two or more (out of a maximum possible of four) associated silicon microvertex detector hits for photons within its two-layer acceptance, or a minimum number of hits in the CV inner axial wires (for photon polar angles beyond the microvertex two-layer acceptance) that are associated in azimuth to the above cluster. Events for which the primary photon is consistent with a photon conversion are called conversion candidates. Events with conversion candidates are rejected if they have at least 2 tracks, reconstructed from axial-wire hits in CV, with an opening angle in the transverse plane exceeding 45 degrees. This cut removes most of the events having charged tracks which do not arise from a single photon conversion.

- **Cluster extent.** Only clusters containing more than one ECAL block are considered as photon candidates. The primary electromagnetic cluster, combined with any clusters contiguous with it, must be consistent with the cluster size and energy sharing of blocks for a photon coming from near the interaction point. The cluster size varies in both azimuthal and polar angle extent as a function of $|\cos\theta|$. The cluster extent cuts are parametrized in $|\cos\theta|$ accordingly.

- **Forward energy vetoes.** The total energy deposited in each of the left and right forward calorimeters and in each of the left and right SiW calorimeters must be less than 5 GeV. The most energetic gamma-catcher cluster must have an energy of less than 5 GeV. These vetoes serve to ensure that photon candidate events are not accompanied by any event activity in the forward regions.

- **Muon veto.** Events are rejected if there are any muon track segments reconstructed in the barrel or endcap muon chambers, or in the barrel, endcap or pole-tip hadron calorimeters. Events are also rejected if three or more of the outer eight layers of the barrel hadron calorimeter have strips hit in any 45° azimuthal octant. The muon veto is used primarily to remove cosmic ray background.

- **Timing measurement in TOF system for low x_T and conversion candidates.** An electromagnetic cluster is said to have an associated TOF hit if it is matched within 50 mrad in azimuthal angle by a good quality TOF counter signal produced by the photon converting before or in the coil which is located in front of the TOF. A cluster with an associated TOF hit has good timing if the measured arrival time of the photon at the TOF is within 20 ns of the expected time for a photon originating from the interaction point. For all events with a photon conversion candidate in the barrel region $|\cos\theta| < 0.82$ and for events with a low x_T ($0.05 < x_T < 0.1$) non-conversion candidate in the barrel region, we require an associated TOF hit with good timing. For all other events with the primary photon in the barrel region, if there is an associated TOF hit, it must have good timing.

- **Special background vetoes for events with no TOF hit.** If the primary non-conversion candidate photon has no associated TOF hit, three different background vetoes are applied. The first rejects events in which any of the three muon triggers [19] (barrel and two endcaps) were present. This veto removes much of the cosmic ray background. The second looks for a series

of calorimeter clusters at the same r and ϕ as the primary cluster, but at different z. This veto rejects beam halo type backgrounds. The third looks for a series of hits in the outer layers of the hadron calorimeter. This veto rejects both cosmic rays and beam related backgrounds.

Events with a second photon candidate are rejected as background from $e^+e^- \to \gamma\gamma(\gamma)$ whilst retaining acceptance for events with two photons and missing energy if any of the following criteria are satisfied:

- The total energy of the two clusters exceeds $0.9\sqrt{s}$.
- The acoplanarity angle[2] of the two clusters is less than 2.5°.
- The missing momentum vector calculated from the two clusters satisfies $|\cos\theta_{\rm miss}| > 0.9$.
- A third electromagnetic cluster is detected with deposited energy exceeding 300 MeV.
- The transverse momentum of the two photon system does not exceed 0.05 of the beam energy.
- For events with at least one of the two clusters in the region $|\cos\theta| > 0.95$, the variable b_T is less than 0.1, where $b_T = (\sin\theta_1 + \sin\theta_2)|\cos[(\phi_1 - \phi_2)/2]|$. This amounts to a stronger acoplanarity cut for events with at least one forward photon.

For the conversion selection, Figure 1 a) shows the maximum of the angular separation, in θ and ϕ, of the primary photon candidate and the highest p_T track in the event. Overlaid as a histogram is the expected distribution from $\nu\overline{\nu}\gamma(\gamma)$ Monte Carlo, normalized to the integrated luminosity of the OPAL data. The cut at 100 mrad rejects contributions from cosmic rays. For the non-conversion selection, Figure 1 b) shows the difference between the measured TOF timing and that expected for a photon from the interaction point, for events passing all selection criteria or failing only the TOF timing requirement. The seven events outside the accepted region of $\pm$20ns are rejected as cosmics.

3.2 Acoplanar-Photons Event Selection Description

The acoplanar-photons selection has two overlapping regions of kinematic acceptance, in order to retain both sensitivity to low-energy photons and acceptance at large $|\cos\theta|$. These selections are based on analyses previously published by OPAL using data collected at centre-of-mass energies of 130-136 GeV [1]. The analysis presented in this paper has increased acceptance and efficiency relative to the previous OPAL analyses. The selection criteria are summarized below:

- **Angular acceptance and minimum energy.** Events are accepted as candidates if there are at least two electromagnetic clusters with scaled energy, x_γ, exceeding 0.05 in in the polar-angle region $15^\circ < \theta < 165^\circ$ ($|\cos\theta| < 0.966$). In order to retain sensitivity to physics processes producing low-energy photons, the minimum energy requirement is relaxed to 1.5 GeV deposited energy for photon candidates in the polar-angle region $|\cos\theta| < 0.8$. This energy deposition corresponds to a photon with an energy of about 1.75 GeV [6]. These two selections are referred to below as the "standard" and "low-energy" selections, respectively. Background vetoes are applied differently for the two parts of the selection, as described below.

[2]Defined as 180° minus the opening angle in the transverse plane.

- **Charged track veto or photon conversion consistency requirements.** We use selection criteria designed to reject events having tracking information consistent with the presence of at least one charged particle originating from the interaction point. These criteria are designed to retain acceptance for events in which one or both of the photons convert. For the standard selection we use hit information from the central jet-chamber, the vertex drift chamber, and the silicon microvertex detector (for $|\cos\theta| < 0.75$ (0.9) for data taken at $\sqrt{s} =$ 130-136 (161, 172) GeV). These three detectors form independent estimators for the existence of charged particle activity. Events in which charged particle activity is associated in azimuth with both photon candidates are rejected unless the signal is from the jet chamber only or from the microvertex detector only. Events in which only one photon candidate has azimuthally associated charged particle activity are rejected if all (two or three) layers of charged particle detection registered activity. To address possible backgrounds from $e^+e^- \to \ell^+\ell^-\gamma\gamma$, an additional veto requires that there be no reconstructed charged track with transverse momentum exceeding 1 GeV, with associated hits in the axial layers of the vertex chamber, and separated from each of the photon candidates by more than 15°.

  The low energy part of the selection requires that there be no reconstructed charged track in the event with 20 or more reconstructed hits in the central jet-chamber.

- **Cluster extent.** Any photon candidate within the polar angle region $|\cos\theta| < 0.75$ is required to have an angular cluster extent that is less than 250 mrad in both θ and ϕ.

- **Forward energy vetoes.** The forward vetoes described for the single-photon analysis are applied with the same thresholds.

- **Muon veto.** To suppress backgrounds arising from cosmic-ray muon interactions or beam halo muons which can deposit significant energy in the calorimeter, the events must pass the muon veto described for the single-photon analysis. Additionally the special background vetoes described for the single-photon selection are applied to events in which no TOF information is present.

- **Timing measurement in TOF system.** Requirements on time-of-flight (TOF) information are defined separately for the two parts of the kinematic selections. For the low-energy part of the selection, we require that the photon in the barrel region has an associated TOF hit with good timing (as defined for the single-photon analysis in section 3.2). For the standard selection, for events in which both of the photon candidates lie within $|\cos\theta| < 0.82$, at least one of them must have an associated TOF hit with good timing. For all events we reject the event if either of the photon candidates has an associated TOF hit with bad timing. Finally, if there is a charged track associated with a cluster within the polar region $|\cos\theta| < 0.82$, the requirement of an associated TOF hit with good timing is applied.

Acoplanar photons events can be faked by cosmic-ray and beam-halo events in which a muon grazes the electromagnetic calorimeter. Such events can produce large clusters which are split by the clustering algorithm to produce two or more clusters. Since it is difficult to model such backgrounds it is useful to have a great deal of redundancy in the procedures used to reject these contributions. This redundancy is provided by the selection criteria outlined above. Figure 1 c) shows the maximum cluster extent for events in which both photons are in the polar-angle region $|\cos\theta| < 0.75$, where cluster-extent cuts are applied. The shaded histogram shows the cluster-extent distribution for real photons coming from the interaction point. These come dominantly from $e^+e^- \to \gamma\gamma$ events selected by removing the anti-$\gamma\gamma(\gamma)$ cuts (described below). The shaded histogram shows the same distribution for events failing the TOF cuts and (possibly) the special background vetoes. The cut at 250 mrad is indicated by the arrow. Additional suppression of such events, as well as of beam-wall/beam-gas events and

instrumental backgrounds in the overlap and endcap regions, is obtained by imposing the following requirements:

- Events are vetoed if there is a reconstructed charged track with at least 20 hits in the jet chamber and a $|z_0|$ larger than 50 cm, where z_0 is the z coordinate of the point of closest approach of the track to the beamline in the transverse plane.
- Events are vetoed if the total number of ECAL clusters having more than 1 GeV of deposited energy is larger than five.
- If both photons have $|\cos\theta| > 0.75$, the opening angle ψ of the two-photon system is required to satisfy $\cos\psi < 0.98$. Otherwise the requirement is that the azimuthal separation of the two candidate clusters be greater than 2.5°.

Finally, background from $e^+e^- \to \gamma\gamma(\gamma)$ is rejected, whilst retaining acceptance for the signal topology, if any of the following criteria are satisfied:

- The total visible energy of the event exceeds $0.95\sqrt{s}$.
- The acoplanarity angle of the two highest-energy clusters is less than 2.5°.
- The missing momentum vector calculated from the two highest-energy photon candidates satisfies $|\cos\theta_{\rm miss}| > 0.95$.
- The transverse momentum of the two-photon system is less than $0.05E_{\rm beam}$; events having a third photon candidate (with $E_\gamma > 300$ MeV) are rejected unless the three photon system is significantly aplanar (sum of the three opening angles < 350°) and the transverse momentum of the three-photon system exceeds $0.1E_{\rm beam}$.

Figure 1 d) shows the distribution of the acoplanarity angle for events passing all cuts or failing one or both of the total-energy cut and the cut on the scaled transverse momentum of the two-photon system. The OPAL data is shown as solid points with error bars. Overlaid as a histogram is the expected distribution, from $e^+e^- \to \gamma\gamma(\gamma)$ Monte Carlo, normalized to the luminosity of the OPAL data. The cut at 2.5° is indicated.

4 Results

The results of the single-photon and acoplanar-photons selections are given below in sections 4.1 and section 4.2 respectively. In each section, the measured cross-sections for the search topology are given and compared with Standard Model expectations, and the results of the XY and XX searches are then described. Upper limits on $\sigma(e^+e^- \to XY) \cdot BR(X \to Y\gamma)$ and $\sigma(e^+e^- \to XX) \cdot BR^2(X \to Y\gamma)$ are given, respectively. This is done both for the general case of massive X and Y, applicable to conventional supersymmetric models in which $X = \tilde{\chi}^0_2$ and $Y = \tilde{\chi}^0_1$, and also separately for the special case of $M_Y \approx 0$, which applies both to single and pair production of neutralinos in supersymmetric models in which the LSP is a light gravitino and to single and pair production of excited neutrinos. These results are used to set limits on the production of excited neutrinos (ν^*) in a separate paper [36]. For all such limits, the efficiencies were evaluated with the decay length of X set to zero. The efficiencies are unaffected if the decay length is much less than the distance from the interaction point to the electromagnetic calorimeters (≈2 m).

For the single-photon and acoplanar-photons analyses, XY and XX Monte Carlo events were generated at each centre-of-mass energy for a variety of mass points in the kinematically accessible region of the $(M_{\rm X}, M_{\rm Y})$ plane. To set limits for arbitrary $M_{\rm X}$ and $M_{\rm Y}$, the efficiency over the entire $(M_{\rm X}, M_{\rm Y})$ plane is parametrized using the efficiencies calculated at the generated mass points. For the single-photon search topology, the region with $M_{\rm X} + M_{\rm Y} < M_{\rm Z}$ is kinematically accessible at $\sqrt{s} \approx M_{\rm Z}$ and strong limits have already been reported [37]. For the acoplanar-photons search topology, we restrict the search to $M_{\rm X}$ values larger than about $M_{\rm Z}/2$. At lower masses, limits have been reported at $\sqrt{s} \approx M_{\rm Z}$ [38] and possible radiative return to the Z followed by $\rm Z \to XX$ would yield very different event kinematics than those of the signal Monte Carlo events used for this study. For both search topologies, at values of $M_{\rm X} - M_{\rm Y} < 5$ GeV, the estimated efficiency decreases significantly due to event kinematics that yield low photon energies. For that reason no limits are set in this region.

4.1 Single-Photon Results $\gamma(\gamma) + \not\!\!E_T$

After applying the selection criteria of the single-photon selection to the $\sqrt{s}$ = 130-172 GeV data samples, a total of 138 events are selected. The expected non-physics background is 2.3 ± 1.1 events, consisting solely of cosmic ray and beam related backgrounds. This non-physics background has been estimated from events detected out of time and using a visual scan with looser cuts. The expected physics backgrounds from plausible sources, $\rm e^+e^- \to \gamma\gamma(\gamma)$, Bhabha events with initial or final-state radiation and $\rm e^+e^- \to \mu^+\mu^-\gamma$ and $\rm e^+e^- \to \tau^+\tau^-\gamma$, have been evaluated to be less than 0.4 events at 95% confidence level (CL) and are therefore considered to be negligible for the cross-section measurement. For each of the four centre-of-mass energies, Table 1 shows the number of events observed, the number of events expected from the Standard Model process $\rm e^+e^- \to \nu\overline{\nu}\gamma(\gamma)$ evaluated using the KORALZ generator, the NNGG03 generator ($\sqrt{s}$ = 130 and 136 GeV) and the NUNUGPV generator ($\sqrt{s}$ = 161 and 172 GeV), and the number of background events expected from non-physics processes. The estimated efficiency for selecting $\rm e^+e^- \to \nu\overline{\nu}\gamma(\gamma)$ events within the kinematic acceptance of the single-photon selection is also given, as is the corresponding measured $\rm e^+e^- \to \nu\overline{\nu}\gamma(\gamma)$ cross-section within this kinematic acceptance, corrected for detector and selection efficiencies, and subtracting the estimated non-physics background. For both the single-photon and acoplanar-photons selections, efficiency losses due to detector occupancy range from about (3-5)% at the different centre-of-mass energies. Here and elsewhere in this paper, unless otherwise stated, quoted efficiencies include these losses and those due to detector status requirements.

The number of events observed agrees with the number of events expected from $\rm e^+e^- \to \nu\overline{\nu}\gamma(\gamma)$ plus the background. The two Monte Carlo generators give similar results although the KORALZ generator has a systematically lower cross-section than NNGG03/NUNUGPV. Following the discussion in section 2, the KORALZ Monte Carlo sample is used for all subsequent measurements and results concerning the $\rm e^+e^- \to \nu\overline{\nu}\gamma(\gamma)$ process unless explicitly mentioned otherwise.

Systematic errors on the cross-section measurement arising from uncertainties on the electromagnetic calorimeter energy scale and resolution, the description of the detector material and consequent conversion probabilities of photons in the central detector volume and coil, the integrated luminosity measurement, and the detector occupancy estimate, have been considered and evaluated to be negligible with respect to the statistical error. A relative systematic error of 4% is assigned to the cross-section measurement. This uncertainty comes dominantly from the estimated uncertainty on the efficiency based on comparing the different event generators. The modelling of the $\rm e^+e^- \to \nu\overline{\nu}\gamma(\gamma)$ event fraction with a second photon detected in the forward detectors ($|\cos\theta| > 0.984$), and therefore rejected by the forward energy vetoes is expected to be the main reason for the observed efficiency differences reported in Table 1. The cross-sections as a function of centre-of-mass energy are plotted

in Figure 2. The curves show the predicted cross-sections from the KORALZ event generator and the NUNUGPV analytical calculation for the Standard Model process $e^+e^- \to \nu\overline{\nu}\gamma(\gamma)$. The data are generally consistent with the predictions but do not favour either estimate.

In Figure 3a, the scaled energy of the most energetic photon is plotted against the cosine of its polar angle for events in the $\sqrt{s}$=172 GeV sample. The data are distributed as expected from the $e^+e^- \to \nu\overline{\nu}\gamma(\gamma)$ Monte Carlo. Similar agreement is seen for the 130, 136 and 161 GeV data. In Figure 3b the polar angle distribution for the entire $\sqrt{s}$=130-172 GeV sample is shown and agrees with the $e^+e^- \to \nu\overline{\nu}\gamma(\gamma)$ Monte Carlo expectation. If one calculates the mass recoiling against the photon (or against the two-photon system) in these events, one expects a peak in the recoil mass at M_Z, since the $\nu\overline{\nu}$ predominantly comes from the decay of a Z^0. One clearly sees this feature in the data as shown in Figure 4. In general there is also good agreement between data and Monte Carlo in this distribution. However, at $\sqrt{s} = 136$ GeV, there is one event with a measured photon energy of 84 GeV. Its estimated recoil mass is imaginary as the measured energy exceeds the beam energy, and it is shown in the distribution as occuring at zero recoil mass. A careful study of this event shows strong evidence, besides the measured energy, that it comes from a cosmic ray, well out-of-time with respect to the LEP beam crossing. In fact, it is sufficiently out-of-time so as to miss detection in several OPAL detector elements including the TOF system. It is left in the data sample because it passes all the selection criteria. It is not, however, considered to be a good physics event candidate.

The single-photon selection was designed to allow for the presence of a second photon in order to accept events from the $e^+e^- \to \nu\overline{\nu}\gamma\gamma(\gamma)$ process. In the data 12 out of the 138 selected events are considered to be two photon events (i.e., have a second photon with deposited energy exceeding 300 MeV). This is consistent with the expectation of 7.1 events from the KORALZ Monte Carlo. Ten of the 12 events are in common with the acoplanar-photons event selection.

4.1.1 Search for $e^+e^- \to XY$, $X \to Y\gamma$ - General case: $M_Y \geq 0$

Selected events at a given centre-of-mass energy are classified as consistent with a given value of M_X and M_Y if the energy of the most energetic photon falls within the region kinematically accessible to a photon from the process $e^+e^- \to XY$, $X \to Y\gamma$. The kinematic consistency criterion includes allowance for the energy resolution and incurs an inefficiency of less than 2% for all values of X and Y masses while accepting only those Standard Model $e^+e^- \to \nu\overline{\nu}\gamma(\gamma)$ events that are kinematically consistent with a given X and Y mass hypothesis.

The kinematic region with true recoil mass significantly below M_Z has only a small background expectation from Standard Model $e^+e^- \to \nu\overline{\nu}\gamma(\gamma)$, but it may be populated as a result of energy mis-measurement in regions of the detector with poorer energy resolution. We reject events as candidates for XY production if the most energetic photon is in one of the following angular regions, $0.785 < |\cos\theta| < 0.815$ and $|\cos\theta| > 0.94$, and the recoil mass is below 75 GeV. One data event is rejected by this cut compared with 1.4 events expected from the Standard Model $e^+e^- \to \nu\overline{\nu}\gamma(\gamma)$ process. We have studied the effect of further cuts to reduce the Standard Model $e^+e^- \to \nu\overline{\nu}\gamma(\gamma)$ background. We find that a significant improvement in the expected sensitivity can be achieved for small M_Y by accepting only events with recoil mass significantly below M_Z. Events are retained as candidates for small M_Y, defined as $M_Y < 14 + 0.1 M_X$ (GeV), if the measured recoil mass is less than 75 GeV. For the complementary, large M_Y region, $M_Y > 14 + 0.1 M_X$ (GeV), no other cuts are applied. The boundary between the small and large M_Y region was chosen so as to optimise the expected sensitivity[3] for the

[3]The optimisation condition chosen was that the upper limit that one would expect to set, on average, in the absence of new physics contributions should be minimised. This definition has the advantage that it does not require one to specify the cross-section of possible new physics.

combined data sample. For simplicity, the same boundary is applied at each centre-of-mass energy.

The selection efficiencies at each generated grid point for the SUSYGEN Monte Carlo events are shown for $\sqrt{s} = 130$ GeV in Table 2 and for $\sqrt{s} = 172$ GeV in Table 3. The efficiencies at intermediate centre-of-mass energies lie between those shown for these two centre-of-mass energies. These values include the efficiency of the kinematic consistency selection criteria which is higher than 98% at each generated mass point. The number of selected events consistent with each $(M_{\mathrm{X}}, M_{\mathrm{Y}})$ value is shown in Figure 5 and can be compared with the number expected from Standard Model $\mathrm{e^+e^-} \to \nu\overline{\nu}\gamma(\gamma)$ events as shown in Figure 6. The background event described earlier does not survive the kinematic consistency cuts for any kinematically accessible point in the $(M_{\mathrm{X}}, M_{\mathrm{Y}})$ plane. In general there is good agreement, and we proceed to set upper limits at 95% CL on the cross-section times branching ratio $\sigma(\mathrm{e^+e^-} \to \mathrm{XY})\cdot\mathrm{BR}(\mathrm{X} \to \mathrm{Y}\gamma)$. These upper limits are first calculated separately at each centre-of-mass energy, as shown in Figure 7. A combined upper limit on the cross-section times branching ratio at $\sqrt{s}$ of 172 GeV is calculated combining the information from each centre-of-mass energy. The combination is performed assuming a cross-section centre-of-mass energy dependence of β_{X}/s, where β_{X} is the speed of particle X. This combined limit is shown in Figure 8. The upper limits are calculated taking into account the expected number of Standard Model $\mathrm{e^+e^-} \to \nu\overline{\nu}\gamma(\gamma)$ background events estimated from KORALZ using the method described in [39]. The estimated non-physics background is intentionally not taken into account in the limit calculation. The resulting combined upper limits range from 0.31 pb to 1.8 pb.

Systematic errors are due primarily to limited Monte Carlo statistics at the generated $(M_{\mathrm{X}}, M_{\mathrm{Y}})$ points and the uncertainty on the efficiency parametrization across the $(M_{\mathrm{X}}, M_{\mathrm{Y}})$ plane. The combined relative uncertainty on the efficiency is 4%. The effect of this uncertainty on the upper limits is calculated according to [40] and is found to be negligible.

4.1.2 Search for $\mathrm{e^+e^-} \to \mathrm{XY}$, $\mathrm{X} \to \mathrm{Y}\gamma$ - Special case: $M_{\mathrm{Y}} \approx 0$

The above results include the case of $M_{\mathrm{Y}} \approx 0$ that lies within the high mass-difference region in which the expected number of events is small. For example, for $M_{\mathrm{X}} = 100$ GeV, two events are observed compared with an expected contribution from $\nu\overline{\nu}\gamma(\gamma)$ of 0.8 ± 0.1 events. For $M_{\mathrm{X}} = 170$ GeV, no events are observed; the background expectation is 0.10 ± 0.03 events. In this region, the requirement that the recoil-mass be less than 75 GeV eliminates all sources of physics background except a small residual contribution from $\mathrm{e^+e^-} \to \gamma\gamma(\gamma)$; the expected contribution is about 0.01 events and is neglected. The upper limits for the $M_{\mathrm{Y}} \approx 0$ case, as a function of M_{X}, are shown in Figure 9. The resulting combined upper limits on $\sigma(\mathrm{e^+e^-} \to \mathrm{XY}) \cdot \mathrm{BR}(\mathrm{X} \to \mathrm{Y}\gamma)$ range from 0.36 pb to 0.76 pb. Interpretation of these results for the production of excited neutrinos is described in a separate paper [36].

4.2 Acoplanar-Photons $\gamma\gamma(\gamma) + \not{E}_T$

After applying the acoplanar-photons selection criteria to the combined data sample, a total of 11 events are observed. The predictions for the total number of Standard Model $\mathrm{e^+e^-} \to \nu\overline{\nu}\gamma\gamma(\gamma)$ events is 6.3 ± 0.2, based on the KORALZ generator. Non-physics background as well as contributions from other Standard Model processes are negligible. The breakdown of the observed and expected number of events for the different centre-of-mass energies is given in Table 4. Within the kinematic acceptance, the selection efficiency[4] for $\mathrm{e^+e^-} \to \nu\overline{\nu}\gamma\gamma(\gamma)$ events is rather constant as a function of centre-of-mass

[4]Before accounting for efficiency losses due to detector occupancy and detector status requirements.

energy, varying from about (67-70)% for the KORALZ generator and from (67-72)% for NNGG03 and NUNUGPV. The mean efficiencies are $(68.6 \pm 1.5)\%$ for KORALZ and $(70.4 \pm 0.5)\%$ for NNGG03 and NUNUGPV. As the cross-section measurements are statistics limited, an efficiency of $(69 \pm 3)\%$ is used independent of $\sqrt{s}$. Additional systematic errors arise due to the energy scale for low-energy photons (5%), and from uncertainty on the luminosity measurement ($< 1\%$). The measured cross-sections for the process $e^+e^- \to \nu\overline{\nu}\gamma\gamma(\gamma)$, within the kinematic acceptance defined by the energy and polar angle selection criteria described earlier, are included in Table 4 as are the cross-section predictions from the KORALZ generator.

There were no selected events having $N_\gamma > 2$, compared with an expectation from KORALZ of 0.34 ± 0.06 events. The kinematic properties of the selected events are summarized in Table 5 and displayed in Figures 10-13 where they are compared with the predicted distributions for $e^+e^- \to \nu\overline{\nu}\gamma\gamma(\gamma)$, obtained using the KORALZ generator, normalized to the corresponding integrated luminosity. Figure 10 shows the recoil-mass distributions of the selected acoplanar-photon pairs. These are peaked near the mass of the Z^0 as expected for contributions from $e^+e^- \to \nu\overline{\nu}\gamma\gamma(\gamma)$. The resolution of the recoil mass is typically about 2-3 GeV at each centre-of-mass energy for $M_{\rm recoil} \approx M_Z$. Figure 11 shows the x_2 vs. x_1 distributions for each centre-of-mass energy and for the combined data sample. The projections of the scaled energy of the least-energetic photon are given in in Figure 12. Figure 13 shows the distributions of the invariant mass, $M_{\gamma\gamma}$, for the selected acoplanar-photon pairs at each centre-of-mass energy. The mass resolution is typically 0.6-1.4 GeV. A search for $H^0 \to \gamma\gamma$ has been recently published by OPAL [17].

For the data at $\sqrt{s} = 161$, 172 GeV, the measured distributions agree with the $\nu\overline{\nu}\gamma\gamma(\gamma)$ expectation. For the $\sqrt{s} = 130, 136$ GeV data there is an apparent excess of events. However, with the exception of the x_2 distribution in Figure 12, for which the measured distribution peaks more strongly than expected at low values, the distributions appear consistent in shape with the expectation from $e^+e^- \to \nu\overline{\nu}\gamma\gamma(\gamma)$. This excess was also remarked on in a previous publication [1].

4.2.1 Search for $e^+e^- \to XX$, $X \to Y\gamma$ - General case: $M_Y \geq 0$

Selected events are classified as consistent with a given value of M_X and M_Y if each of the two selected photons falls within the region kinematically accessible to photons from the process $e^+e^- \to XX$, $X \to Y\gamma$. As before, this includes allowance for resolution effects. Monte Carlo events were generated at each centre-of-mass energy. The selection efficiencies at each generated grid point for the $\sqrt{s} = 172$ GeV SUSYGEN Monte Carlo events are shown in Table 6. These values include the efficiency of the kinematic consistency selection criteria which is higher than 95% at each generated point in the (M_X, M_Y) plane. Similar efficiencies are obtained at the other centre-of-mass energies.

Figures 14 (a)-(d) show the 95% CL $\sigma(e^+e^- \to XX) \cdot BR^2(X \to Y\gamma)$ exclusion plots obtained at $\sqrt{s} = 130$, 136, 161 and 172 GeV respectively. Because of the current uncertainties on the modelling of the Standard Model background, as discussed earlier, these limits and the limits presented below for this topology, have been calculated without taking into account the background estimate. Events from $e^+e^- \to \nu\overline{\nu}\gamma\gamma(\gamma)$ are typically characterized by a high-energy photon from the radiative return to the Z^0 and a second lower energy photon. The kinematic consistency requirements, however, require that the two photons have energies within the same (kinematically accessible) region. For this reason, two of the selected events are inconsistent with any (M_X, M_Y) point for $M_X \geq 45$ GeV and $M_X - M_Y \geq 5$ GeV. Figure 15 shows the 95% CL $\sigma(e^+e^- \to XX) \cdot BR^2(X \to Y\gamma)$ exclusion plot obtained from the combined data sample assuming that $\sigma(e^+e^- \to XX)$ scales with centre-of-mass energy as β_X/s. For the combined plot, the maximum value of the limit is 0.80 pb. The minimum value is 0.18 pb.

Systematic errors are due primarily to limited Monte Carlo statistics at the generated (M_X, M_Y) points and the uncertainty on the efficiency parametrization across the (M_X, M_Y) plane. The combined relative uncertainty on the efficiency varies from about (3-6)% across the plane. All systematic uncertainties are accounted for in the manner advocated in reference [40]. This also applies to the limits for the $M_Y \approx 0$ case, presented in the next section.

4.2.2 Search for $e^+e^- \to XX$, $X \to Y\gamma$ - Special case: $M_Y \approx 0$

For the special case of $M_Y \approx 0$ the kinematic consistency cuts applied differ from those used for the general case. One can calculate [14] the maximum and minimum masses, M_X^{max} and M_X^{min}, which are consistent with the kinematic properties of the two photons, assuming a massless Y. As this argument is based only on kinematics it applies generally to the case where the acoplanar photon pair originates from pair production of heavy neutral particles which decay radiatively to massless invisible final states; $e^+e^- \to XX$ followed by $X \to Y\gamma$, $M_Y \approx 0$. These maximum and minimum mass values can provide further suppression of the $\nu\overline{\nu}\gamma\gamma(\gamma)$ background while retaining high efficiency for the signal hypothesis. The background suppression achieved with kinematic consistency requirements based on this procedure is much better than that obtained for the general case since, in this case, the full event kinematics are used. Figure 16 shows M_X^{min} vs. M_X^{max} for events passing the selection criteria described in section 3.2 for, (a) $\nu\overline{\nu}\gamma\gamma(\gamma)$ Monte Carlo and (b-d) $e^+e^- \to XX$, $X \to Y\gamma$, $M_Y \approx 0$ signal Monte Carlo, at $\sqrt{s} = 172$ GeV, for three values of M_X. The signal Monte Carlo distributions are dominantly populated at maximum mass values greater than or equal to the generated mass of X (e.g. ν^* or $\tilde{\chi}_1^0$). Resolution effects shift some entries to lower masses. Requiring that the maximum kinematically allowed mass be greater than $M_X - 5$ GeV retains more than 95% relative efficiency for signal at all values of M_X while suppressing 41% to 96% of the remaining $\nu\overline{\nu}\gamma\gamma(\gamma)$ events. Similar efficiencies are obtained at each of the other centre-of-mass energies.

The kinematic properties of the selected events, shown in Table 5, include the values of M_X^{max}. The data distributions in M_X^{min} vs. M_X^{max} are shown for each of the centre-of-mass energies in Figure 17. In each case the distribution for $\nu\overline{\nu}\gamma\gamma(\gamma)$ events is also shown. For illustrative purposes, the efficiencies calculated from Monte Carlo events generated at 172 GeV are shown in Table 7 before and after application of the cut on M_X^{max}. Also shown is the $\nu\overline{\nu}\gamma\gamma(\gamma)$ rejection efficiency obtained with the M_X^{max} cut. Signal efficiencies at other centre-of-mass energies are similar.

Based on the efficiencies and the number of events observed at each centre-of-mass energy, we calculate 95% CL upper limits on $\sigma(e^+e^- \to XX) \cdot BR^2(X \to Y\gamma)$ (for $M_Y \approx 0$) as a function of M_X. These are shown in Figure 18. Also shown is the 95% CL upper limit obtained from the combined data sample, assuming a centre-of-mass energy dependence of the cross-section of β_X/s. This combined limit is 0.5 pb or less for values of M_X from 45 GeV up to the kinematic limit.

To set combined, model dependent limits on the mass of the $\tilde{\chi}_1^0$ (NLSP) in supersymmetric models in which the LSP is a light gravitino, we sum the number of observed events consistent with each value of M_X. This distribution is shown in Figure 19 where the solid line shows the number of observed candidates consistent with a given value of M_X and the dashed-dotted line shows the background expectation from KORALZ. The number of candidate events is consistent with the number of background events expected from $\nu\overline{\nu}\gamma\gamma(\gamma)$. The thick solid line shows the 95% confidence level upper limit at each mass value. The background expectation is not taken into account when calculating the limit. Also shown in Figure 19 are the numbers of events expected from the Lopez and Nanopoulos no-scale supergravity model [14] and from the model of Babu, Kolda and Wilczek [16] in which the neutralino composition is purely gaugino (bino). For both of these models, the cross-section has been evaluated

at Born level. Based on these distributions, these two models are ruled out at the 95% confidence level for $M_{\tilde{\chi}^0_1} < 61.3$ GeV and 69.4 GeV, respectively.

As described above, the efficiencies over the full angular range have been calculated using isotropic angular distributions for production and decay of X. The validity of this model has been examined based on the angular distributions calculated for photino pair production in [12]. For models proposed in [13], the production angular distributions are more central and so this procedure is conservative. For a $1 + \cos^2\theta$ production angular distribution, expected for t-channel exchange of a very heavy particle according to [12], the relative efficiency reduction would be less than 2% for all points in the $M_{\rm X}, M_{\rm Y}$ plane (for $M_{\rm X} - M_{\rm Y} > 5$ GeV).

Interpretation of these results for the production of excited neutrinos is described in a separate paper [36].

5 Conclusions

We have searched for photonic events with large missing energy in two different and complementary topologies in data taken with the OPAL detector at LEP, at centre-of-mass energies in the region of 130-172 GeV.

In the single-photon selection which requires at least one photon with $x_T > 0.05$ in the region $|\cos\theta| < 0.82$ or one photon with $x_T > 0.1$ in the region $15^\circ < \theta < 165^\circ$ ($|\cos\theta| < 0.966$) a total of 138 events are observed in the data compared to the KORALZ prediction for the contribution from the Standard Model process $\mathrm{e^+e^-} \to \nu\overline{\nu}\gamma(\gamma)$ of 141.1 ± 1.1 events and an expected non-physics background of 2.3 ± 1.1 events. The corresponding cross-sections for $\mathrm{e^+e^-} \to \nu\overline{\nu}\gamma(\gamma)$ are 10.0 ± 2.3, 16.3 ± 2.8, 5.3 ± 0.8 and 5.5 ± 0.8 pb for $\sqrt{s} = 130$, 136, 161 and 172 GeV, respectively, in agreement with the Standard Model expectations. We derive upper limits on the cross-section times branching ratio for the process $\mathrm{e^+e^-} \to \mathrm{XY}$, $\mathrm{X} \to \mathrm{Y}\gamma$ for the general case of massive X and Y. The limits vary from 0.31 to 1.8 pb in the region of interest of the $(M_{\rm X}, M_{\rm Y})$ plane and include the special case of $M_{\rm Y} \approx 0$, where the limit varies between 0.36 and 0.76 pb for the $M_{\rm X}$ mass range from $M_{\rm Z}$ to 172 GeV.

The acoplanar-photons selection requires at least two photons with scaled energy $x_\gamma > 0.05$ within the polar angle region $15^\circ < \theta < 165^\circ$ or at least two photons with energy $E_\gamma > 1.75$ GeV with one satisfying $|\cos\theta| < 0.8$ and the other satisfying $15^\circ < \theta < 165^\circ$. From the combined data sample 11 events are selected. The KORALZ prediction for the number of events from $\mathrm{e^+e^-} \to \nu\overline{\nu}\gamma\gamma(\gamma)$ is 6.3 ± 0.2. The cross-section for this process is measured at each centre-of-mass energy (see Table 4). Due to the uncertainties in the current modelling of the Standard Model background, $\mathrm{e^+e^-} \to \nu\overline{\nu}\gamma\gamma(\gamma)$, all limits from the acoplanar-photons analysis were calculated without taking into account the background estimate. Based on a variety of kinematic distributions, all observed events appear consistent with $\mathrm{e^+e^-} \to \nu\overline{\nu}\gamma\gamma(\gamma)$. We derive 95% CL upper limits on $\sigma(\mathrm{e^+e^-} \to \mathrm{XX}) \cdot \mathrm{BR}^2(\mathrm{X} \to \mathrm{Y}\gamma)$ ranging from 0.18 to 0.80 pb for the general case of massive X and Y, and from 0.35 to 0.50 pb for the special case of $M_{\rm Y} \approx 0$.

For the single-photon and acoplanar-photons search topologies, the general case of massive X and Y is relevant to the supersymmetry models in which $\mathrm{X} = \tilde{\chi}^0_2$ and $\mathrm{Y} = \tilde{\chi}^0_1$, with $\tilde{\chi}^0_2 \to \tilde{\chi}^0_1\gamma$ and $\tilde{\chi}^0_1$ stable. The special case of $M_{\rm Y} \approx 0$ is of particular interest for single and pair production of excited neutrinos and for supersymmetric models in which the LSP is a light gravitino and the $\tilde{\chi}^0_1$ is the NLSP which decays as $\tilde{\chi}^0_1 \to \tilde{\mathrm{G}}\gamma$. For the latter scenario, the results of the acoplanar-photons search are

used to place model-dependent lower limits on the $\tilde{\chi}_1^0$ mass. Comparison with the model predictions of Lopez and Nanopoulos [14] permits exclusion of that model for $M_{\tilde{\chi}_1^0} < 61.3$ GeV. A similar model from Babu, Kolda and Wilczek [16] is excluded for $M_{\tilde{\chi}_1^0} < 69.4$ GeV. The results of these searches have also been used to place limits on the production of excited neutrinos [36].

6 Acknowledgements

The authors wish to thank J.L. Lopez for providing cross-section results, and S. Ambrosanio, G.Kane, G. Montagna and Z. Wąs for useful discussions on the estimation of the Standard Model cross-sections.

We particularly wish to thank the SL Division for the efficient operation of the LEP accelerator at all energies and for their continuing close cooperation with our experimental group. We thank our colleagues from CEA, DAPNIA/SPP, CE-Saclay for their efforts over the years on the time-of-flight and trigger systems which we continue to use. In addition to the support staff at our own institutions we are pleased to acknowledge the
Department of Energy, USA,
National Science Foundation, USA,
Particle Physics and Astronomy Research Council, UK,
Natural Sciences and Engineering Research Council, Canada,
Israel Science Foundation, administered by the Israel Academy of Science and Humanities,
Minerva Gesellschaft,
Benoziyo Center for High Energy Physics,
Japanese Ministry of Education, Science and Culture (the Monbusho) and a grant under the Monbusho International Science Research Program,
German Israeli Bi-national Science Foundation (GIF),
Bundesministerium für Bildung, Wissenschaft, Forschung und Technologie, Germany,
National Research Council of Canada,
Research Corporation, USA,
Hungarian Foundation for Scientific Research, OTKA T-016660, T023793 and OTKA F-023259.

References

[1] OPAL Collab., G. Alexander et al., Phys. Lett. **B377** (1996) 222.

[2] OPAL Collab., K. Ackerstaff et al., Phys. Lett. **B391** (1997) 210.

[3] OPAL Collab., G. Alexander et al., Phys. Lett. **B386** (1996) 463.

[4] OPAL Collab., K. Ackerstaff et al., Phys. Lett. **B391** (1997) 197.

[5] OPAL Collab., K. Ackerstaff et al., CERN-PPE/97-109, submitted to Zeit. Phys. **C**.

[6] OPAL Collab., R. Akers et al., Z. Phys. **C65** (1995) 47.

[7] L3 Collab., B. Adeva et al., Phys. Lett. **B275** (1992) 209;
L3 Collab., O. Adriani et al., Phys. Lett. **B292** (1992) 463;
ALEPH Collab., D. Buskulic et al., Phys. Lett. **B313** (1993) 520;
DELPHI Collab., P. Abreu et al., Z. Phys. **C74** (1997) 577.

[8] MAC Collab., W.T. Ford et al., Phys. Rev. **D33** (1986) 3472;
H. Wu, Ph.D Thesis, Univ. Hamburg, 1986;
CELLO Collab., H.-J. Behrend et al., Phys. Lett. **B215** (1988) 186;
ASP Collab., C. Hearty et al., Phys. Rev. **D39** (1989) 3207;
VENUS Collab., K. Abe et al., Phys. Lett. **B232** (1989) 431;
TOPAZ Collab., T. Abe et al., Phys. Lett. **B361** (1995) 199.

[9] ALEPH Collab., D. Buskulic et al., Phys. Lett. **B384** (1996) 333;
L3 Collab., M. Acciarri et al., Phys. Lett. **B384** (1996) 323;
DELPHI Collab., P. Abreu et al., Phys. Lett. **B380** (1996) 471;
L3 Collab., M. Acciarri et al., CERN-PPE/97-76, submitted to Phys. Lett. **B**;
ALEPH Collab., R.Barate et al., CERN-PPE/97-122, submitted to Phys. Lett. **B**.

[10] S. Ambrosanio et al., Phys. Rev. Lett. **76** (1996) 3498; Phys. Rev. **D55** (1997) 1392.

[11] H.E. Haber and D. Wyler, Nucl. Phys. **B323** (1989) 267;
S. Ambrosanio and B. Mele, Phys. Rev. **D53** (1996) 2541.

[12] J. Ellis and J.S. Hagelin, Phys. Lett. **B122** (1983) 303.

[13] S. Dimopoulos et al., Phys. Rev. Lett. **76** (1996) 3494;
D.R. Stump, M. Wiest, C.P. Yuan, Phys. Rev. **D54** (1996) 1936;
S. Ambrosanio et al., Phys. Rev. **D54** (1996) 5395.

[14] J.L. Lopez and D.V. Nanopoulos, Mod. Phys. Lett. **A11** (1996) 2473; Phys. Rev. **D55** (1997) 4450.

[15] J.L. Lopez, D.V. Nanopoulos, A. Zichichi, Phys. Rev. Lett. **77** (1996) 5168.

[16] C.Y. Chang and G.A. Snow, UMD/PP/97-57.
K. S. Babu, C. Kolda and F. Wilczek, Phys. Rev. Lett. **77** (1996) 3070.

[17] OPAL Collab, K. Ackerstaff et al., CERN-PPE/97-121, submitted to Z. Phys. **C**.

[18] OPAL Collab., K. Ahmet et al., Nucl. Instrum. Methods **A305** (1991) 275;
P.P. Allport et al., Nucl. Instrum. Methods **A324** (1993) 34;
P.P. Allport et al., Nucl. Instrum. Methods **A346** (1994) 476;
B.E. Anderson et al., IEEE Transactions on Nuclear Science **41** (1994) 845.

[19] M. Arignon et al., Nucl. Instrum. Methods **A313** (1992) 103.

[20] F.A. Berends et al., Nucl. Phys. **B301** (1988) 583;
R. Miquel, C. Mana and M. Martinez, Z. Phys. **C48** (1990) 309.

[21] G. Montagna et al., Nucl. Phys. **B452** (1996) 161;
G. Montagna, O. Nicrosini and F. Piccinini, FNT/T-96/1, to be published in Comp. Phys. Comm.

[22] S. Jadach et al., Comp. Phys. Comm. **66** (1991) 276. Version 4.02 was used including a recommended correction to the NDIST0 subroutine.

[23] F.A. Berends and R. Kleiss, Nucl. Phys. **B186** (1981) 22.

[24] S. Jadach, W. Placzek and B. F. L. Ward, Phys. Lett. **B390** (1997) 398.

[25] D. Karlen, Nucl. Phys. **B289** (1987) 23.

[26] S. Katsanevas and S. Melachronios, CERN/96-01, Vol.2 (1996) 328.

[27] J. Allison et al., Nucl. Instrum. Methods **A317** (1992) 47.

[28] P. Colas, R. Miquel and Z. Wąs, Phys. Lett. **B246** (1990) 541.

[29] D. R. Yennie, S. C. Frautschi and H. Suura, Annals of Phys. **13** (1961) 379.

[30] E. E. Boos et al., "COMPHEP: Specialized Package for Automatic Calculations of Elementary Particle Decays and Collisions", SNUTP-94-116.

[31] S. Ambrosanio, G. D. Kribs and S. P. Martin, Phys. Rev. **D56** (1997) 1761.

[32] H. Murayama et al., "HELAS: Helicity Amplitude Subroutines for Feynman Diagram Evaluations", KEK 91-11 (1992).

[33] S. Mrenna, "Physics Backgrounds to Supersymmetric Signals with Two Photons and Missing Mass at LEP", ANL-HEP-PR-97-27.

[34] P. Bain and R. Pain, "Acoplanar Photons Background Generators", Contributed paper number 528, EPS conference, Jerusalem, 1997.

[35] MINAMI-TATEYA group, "GRACE Manual: Automatic Generation of Tree Amplitudes in Standard Models, Version 1.0", KEK report 92-19 (1993).

[36] OPAL Collab., K. Ackerstaff et al., CERN-PPE/97-123, submitted to Z. Phys. **C**.

[37] L3 Collab., M. Acciarri et al., Phys. Lett. **B350** (1995) 109;
OPAL Collab., G. Alexander et al., Phys. Lett. **B377** (1996) 273.

[38] OPAL Collab., M.Z. Akrawy et al., Phys. Lett. **B248** (1990) 211;
ALEPH Collab., D. Decamp et al., Phys. Rep. 216 (1992) 253;
L3 Collab., M. Acciarri et al., Phys. Lett. **B350** (1995) 109.

[39] Particle Data Group, R. M. Barnett et al., Phys. Rev. **D54** (1996) 1.

[40] R. D. Cousins and V. L. Highland, Nucl. Instrum. Methods **A320** (1992) 331.

$\sqrt{s}$(GeV)	N_{obs}	$N_K^{\nu\overline{\nu}\gamma(\gamma)}$	$N_N^{\nu\overline{\nu}\gamma(\gamma)}$	N_{bkg}	$\epsilon_K^{\nu\overline{\nu}\gamma(\gamma)}$(%)	$\epsilon_N^{\nu\overline{\nu}\gamma(\gamma)}$(%)	$\sigma_{meas}^{\nu\overline{\nu}\gamma(\gamma)}$(pb)
130	19	25.3 ± 0.4	27.5 ± 0.3	0.2 ± 0.2	81.6 ± 0.6	79.6 ± 0.5	10.0 ± 2.3
136	34	23.3 ± 0.4	25.8 ± 0.3	0.3 ± 0.2	79.7 ± 0.7	80.0 ± 0.5	16.3 ± 2.8
161	40	48.3 ± 0.6	51.3 ± 0.4	0.9 ± 0.8	75.2 ± 0.5	72.3 ± 0.4	5.3 ± 0.8
172	45	44.3 ± 0.6	46.1 ± 0.4	0.9 ± 0.8	77.9 ± 0.5	74.5 ± 0.4	5.5 ± 0.8
130-172	138	141.2 ± 1.1	150.7 ± 0.7	2.3 ± 1.1			

Table 1: For each centre-of-mass energy, the table shows the number of events observed in the OPAL data, the number expected based on the KORALZ (K) and NUNUGPV/NNGG03 (N) $e^+e^- \to \nu\overline{\nu}\gamma(\gamma)$ event generators and the number of events expected from non-physics backgrounds. Also shown are the efficiencies obtained from the two generators, within the kinematic acceptance of the single-photon selection, and the measured cross-sections within the kinematic acceptance, determined using the efficiencies obtained with the KORALZ generator. The quoted cross-section errors are statistical.

$M_X + M_Y$	$M_Y = 0$	$M_Y = M_X/2$	$M_Y = M_X - 15$ GeV	$M_Y = M_X - 5$ GeV
110	80.2 ± 1.7	83.7 ± 1.5	80.9 ± 1.7	51.3 ± 2.2
120	82.3 ± 1.6	86.6 ± 1.4	80.2 ± 1.7	49.2 ± 2.2
128	84.9 ± 1.5	84.4 ± 1.5	82.5 ± 1.6	49.6 ± 2.2

Table 2: Single photon selection efficiency (%) as a function of the sum of M_X and M_Y versus various M_Y values for the process $e^+e^- \to XY$, $X \to Y\gamma$. These efficiencies are for $\sqrt{s} = 130$ GeV. Masses given are in GeV.

$M_X + M_Y$	$M_Y = 0$	$M_Y = M_X/2$	$M_Y = M_X - 15$ GeV	$M_Y = M_X - 5$ GeV
110	23.4 ± 1.3	83.5 ± 1.1	75.8 ± 1.3	38.5 ± 1.5
130	32.1 ± 1.4	86.4 ± 1.0	74.6 ± 1.3	36.5 ± 1.5
150	65.6 ± 1.4	85.0 ± 1.0	75.3 ± 1.3	32.2 ± 1.5
160	80.0 ± 1.2	86.5 ± 1.0	74.0 ± 1.3	30.9 ± 1.4
170	82.9 ± 1.1	88.7 ± 0.9	74.8 ± 1.3	30.8 ± 1.4

Table 3: Single photon selection efficiency (%) as a function of the sum of M_X and M_Y versus various M_Y values for the process $e^+e^- \to XY$, $X \to Y\gamma$. These efficiencies are for $\sqrt{s} = 172$ GeV. Masses given are in GeV. The errors are statistical.

$\sqrt{s}$(GeV)	$\mathcal{L}$(pb^{-1})	N_{obs}	$N_{exp}^{\nu\overline{\nu}\gamma\gamma(\gamma)}$	$\sigma^{\nu\overline{\nu}\gamma\gamma(\gamma)}$(pb)	$\sigma_{exp}^{\nu\overline{\nu}\gamma\gamma(\gamma)}$(pb)
130	2.30	3	0.83 ± 0.08	2.0 ± 1.1	0.54 ± 0.04
136	2.59	5	0.77 ± 0.08	3.0 ± 1.3	0.48 ± 0.04
161	9.89	1	2.41 ± 0.15	0.16 ± 0.16	0.35 ± 0.02
172	10.28	2	2.28 ± 0.15	0.30 ± 0.21	0.33 ± 0.02
130-172	25.06	11	6.29 ± 0.24		

Table 4: Number of acoplanar-photons events observed and expected at each centre-of-mass energy region and the corresponding measured and expected (KORALZ) cross-sections within the kinematic acceptance of the acoplanar-photons event selection.

$\sqrt{s}$(GeV)	x_1	x_2	cosθ_1	cosθ_2	ϕ_1(rad)	ϕ_2(rad)	$M_{\rm recoil}$	$M_{\gamma\gamma}$	$M_{\rm X}^{\rm max}$
130.3	0.313	0.048	0.785	-0.721	5.134	0.095	105.0	13.5	20.6
130.3	0.435	0.276	0.473	-0.926	4.064	1.172	81.9	42.3	51.7
130.3	0.449	0.091	0.484	0.166	2.147	4.574	91.4	23.3	25.6
136.2	0.499	0.069	-0.800	0.024	0.377	2.642	92.0	21.2	24.8
136.2	0.529	0.036	-0.154	-0.506	4.105	4.799	90.2	6.8	24.8
136.2	0.456	0.150	0.420	0.896	0.692	3.408	91.8	33.2	32.1
136.2	0.512	0.031	-0.231	-0.026	5.845	4.147	93.0	12.9	18.2
136.2	0.515	0.070	0.465	0.413	1.413	2.484	88.5	11.9	34.0
161.3	0.402	0.166	0.580	0.095	1.206	0.581	107.2	15.8	59.6
172.3	0.592	0.170	0.046	0.787	5.509	3.776	93.0	39.9	58.8
172.3	0.565	0.209	0.901	-0.269	1.510	2.866	93.5	44.9	64.7

Table 5: Kinematic properties of the events passing the acoplanar-photons selection. All masses are given in GeV. $M_{\rm X}^{\rm max}$ is defined in Section 4.2.2.

$M_{\rm X}$	$M_{\rm Y}$=0	$M_{\rm Y} = M_{\rm X}/2$	$M_{\rm Y} = M_{\rm X} - 15$ GeV	$M_{\rm Y} = M_{\rm X} - 5$ GeV
85	72.6 ± 1.3	71.0 ± 1.3	69.1 ± 1.4	43.2 ± 1.5
80	72.6 ± 1.3	73.3 ± 1.3	71.1 ± 1.3	41.2 ± 1.5
75	73.6 ± 1.3	72.6 ± 1.3	69.7 ± 1.4	39.9 ± 1.4
70	71.8 ± 1.3	69.2 ± 1.4	68.9 ± 1.4	42.3 ± 1.5
55	68.1 ± 1.4	67.7 ± 1.4	65.8 ± 1.4	41.8 ± 1.5
45	67.3 ± 1.4	66.1 ± 1.4	64.2 ± 1.4	40.6 ± 1.4

Table 6: Acoplanar-photons selection efficiencies (%) for the process $e^+e^- \to XX$, $X \to Y\gamma$ at $\sqrt{s} = 172$ GeV for various $M_{\rm X}$ and $M_{\rm Y}$ (in GeV). These values include the efficiency of the kinematic consistency cuts. Similar efficiencies are obtained at each value of $\sqrt{s}$. The errors are statistical.

$M_{\rm X}$	Selection efficiency for $e^+e^- \to XX$, $X \to Y\gamma$	Selection efficiency with $M_{\rm X}^{\rm max} > M_{\rm X} - 5$ GeV	$\nu\overline{\nu}\gamma\gamma(\gamma)$ rejection efficiency
85	74.7 ± 1.2	72.5 ± 1.2	95.7 ± 1.3
80	74.5 ± 1.2	70.7 ± 1.3	89.7 ± 2.0
75	74.9 ± 1.2	72.7 ± 1.2	85.4 ± 2.3
70	72.7 ± 1.2	69.6 ± 1.3	79.4 ± 2.7
55	68.7 ± 1.3	66.1 ± 1.3	58.4 ± 3.2
45	68.1 ± 1.3	64.8 ± 1.4	41.2 ± 3.2

Table 7: Acoplanar-photons event selection efficiency (%), as a function of mass, for the process $e^+e^- \to XX$, $X \to Y\gamma$, for $M_{\rm Y} \approx 0$. These numbers are for $\sqrt{s} = 172$ GeV. The first column shows the efficiency of the selection described in section 3.2. The second column shows the selection efficiency after the cut on $M_{\rm X}^{\rm max}$ described in section 4.2.2. The final column shows the rejection efficiency (%) of the $M_{\rm X}^{\rm max} > M_{\rm X} - 5$ GeV cut for $\nu\overline{\nu}\gamma\gamma(\gamma)$ events. The errors are statistical.

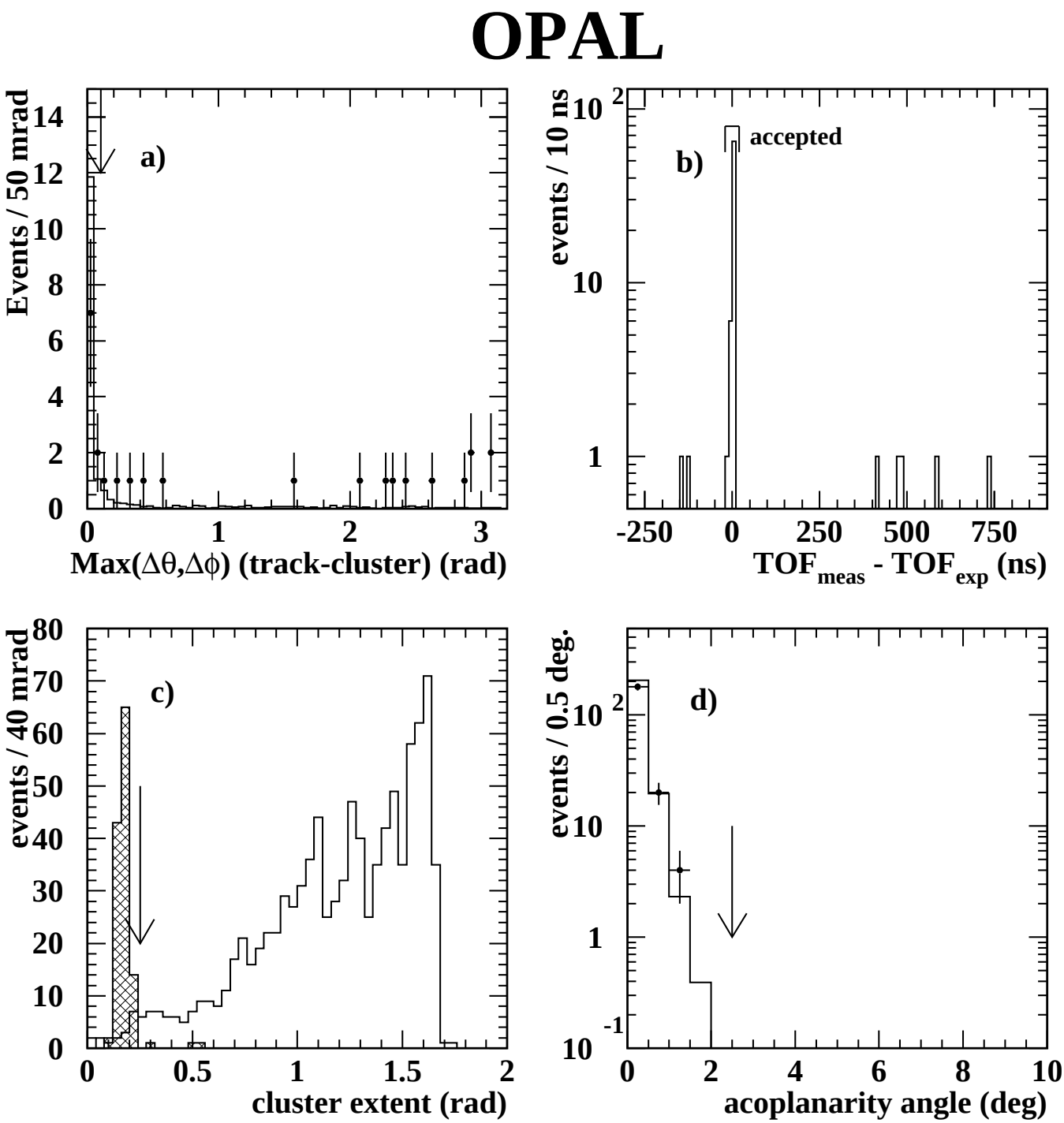

Figure 1: For single-photon conversion candidates, a) shows the maximum angular separation in θ and ϕ of the primary photon candidate and the highest p_T track in the event. For the non-conversion single-photon selection, b) shows the difference between the observed TOF timing and the timing expected for a photon from the interaction point, for data events passing all cuts or failing only the timing cut. For the acoplanar-photons selection, c) shows the maximum cluster extent for data events failing only the anti-$\gamma\gamma(\gamma)$ cuts (shaded histogram) and for data events failing the TOF requirements or the TOF requirement and the special background vetoes (unshaded histogram). For the acoplanar-photons selection, d) shows the distribution of the acoplanarity angle for data events failing only the total energy cut and/or the cut on $p_T(\gamma\gamma)$ (predominantly $e^+e^- \to \gamma\gamma$). In a) and d) the solid points with error bars show the OPAL data while the overlaid histograms represent the expectation from $\nu\overline{\nu}\gamma(\gamma)$ and $e^+e^- \to \gamma\gamma(\gamma)$ Monte Carlo, respectively, normalized to the luminosity of the data.

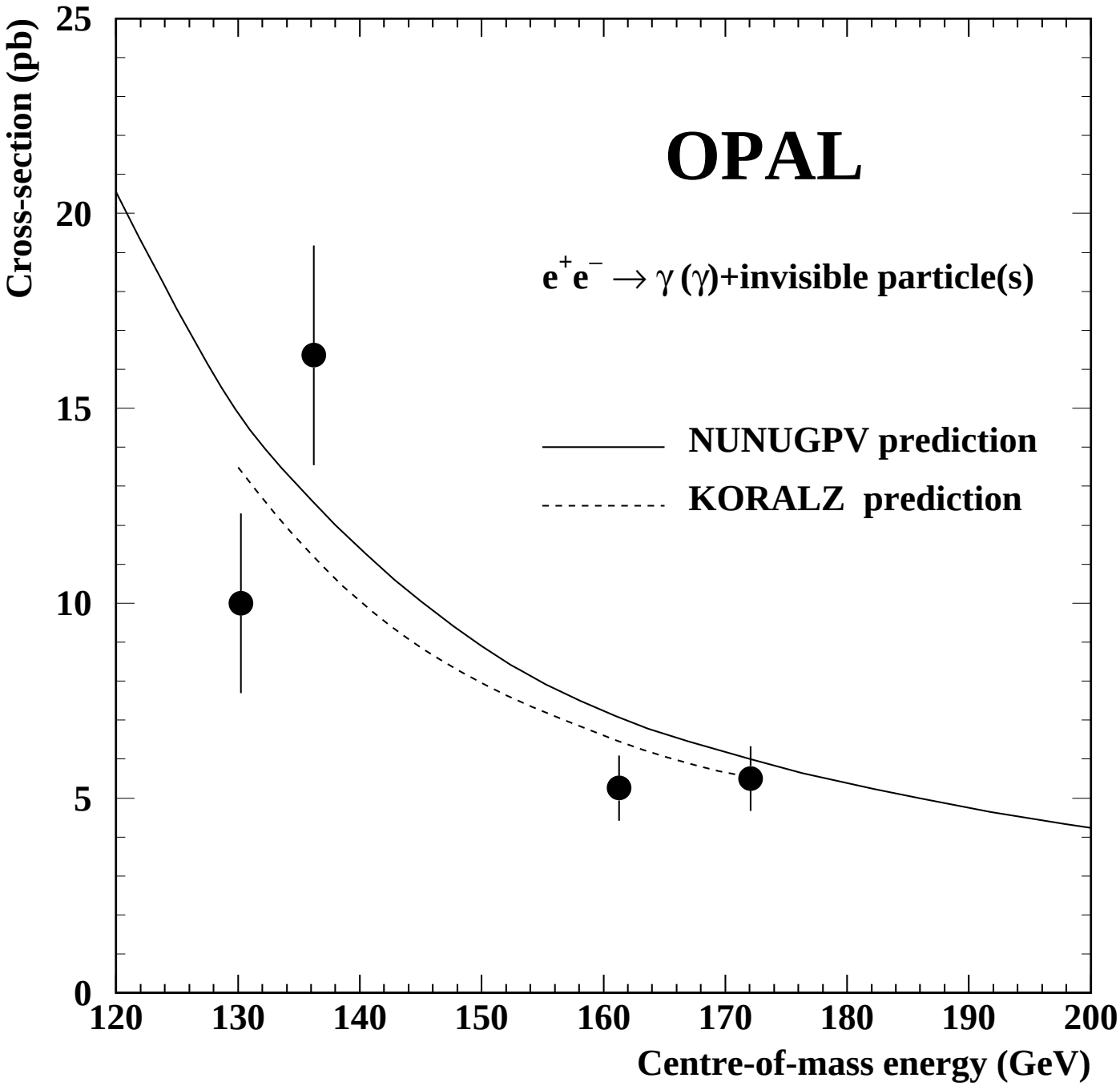

Figure 2: The measured value of $\sigma(e^+e^- \to \gamma(\gamma)$ + invisible particle(s)), within the kinematic acceptance of the single-photon selection, as a function of $\sqrt{s}$. The data points with error bars are OPAL measurements at centre-of-mass energies of 130, 136, 161 and 172 GeV. The curves are the predictions for the Standard Model process $e^+e^- \to \nu\overline{\nu}\gamma(\gamma)$ from the KORALZ generator and the NUNUGPV analytical calculation.

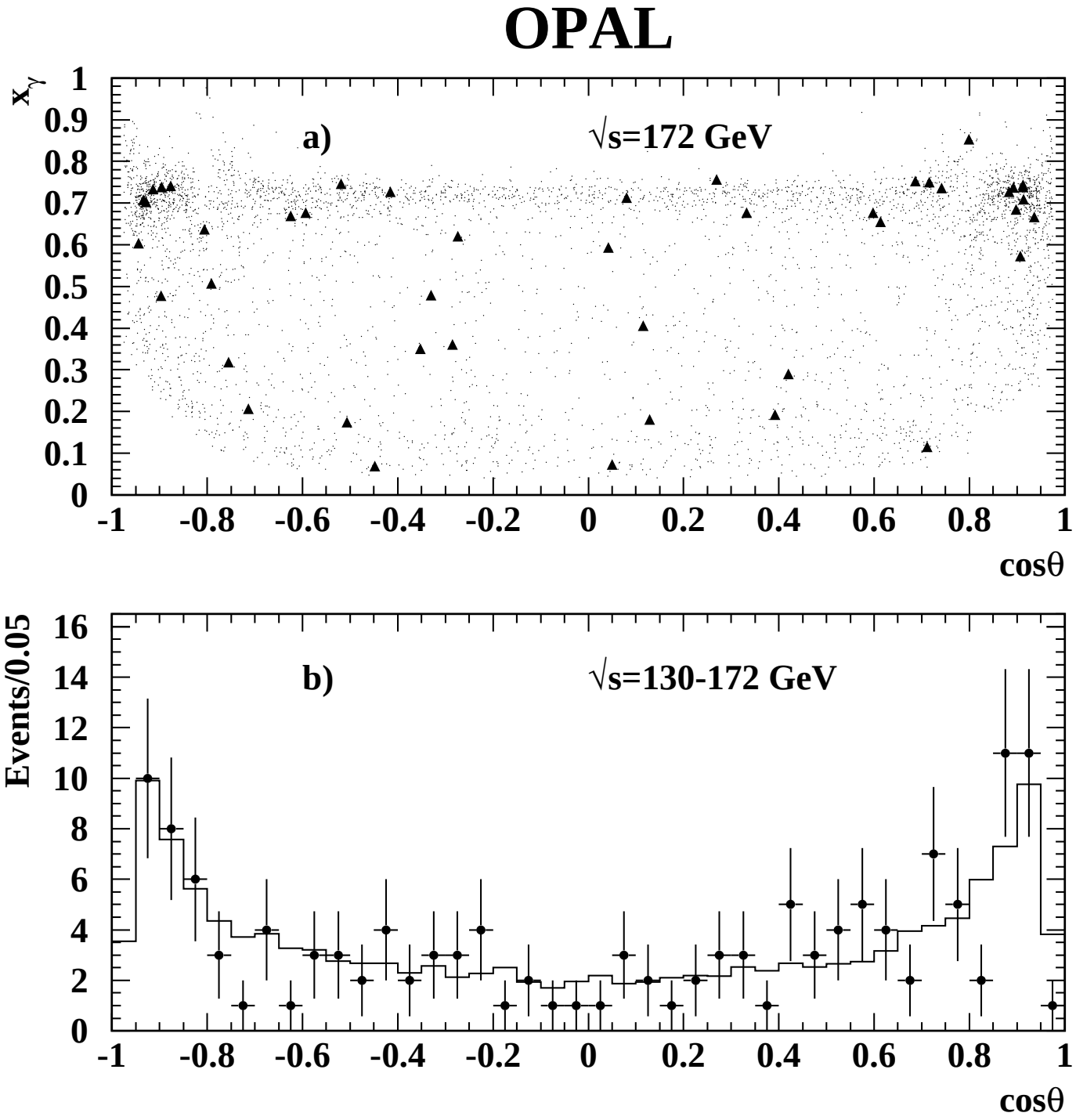

Figure 3: a) Distribution of x_γ vs $\cos\theta$ for the most energetic photon in the single photon selection. The fine points are the KORALZ $e^+e^- \to \nu\overline{\nu}\gamma(\gamma)$ Monte Carlo and the solid triangles are the data. This plot is for $\sqrt{s} = 172$ GeV. b) The $\cos\theta$ distribution for the most energetic photon in the single photon selection. The points with error bars are the data and the histogram is the expectation from the KORALZ $e^+e^- \to \nu\overline{\nu}\gamma(\gamma)$ Monte Carlo normalized to the integrated luminosity of the data. This plot is for the combined data set $\sqrt{s} = 130$-172 GeV.

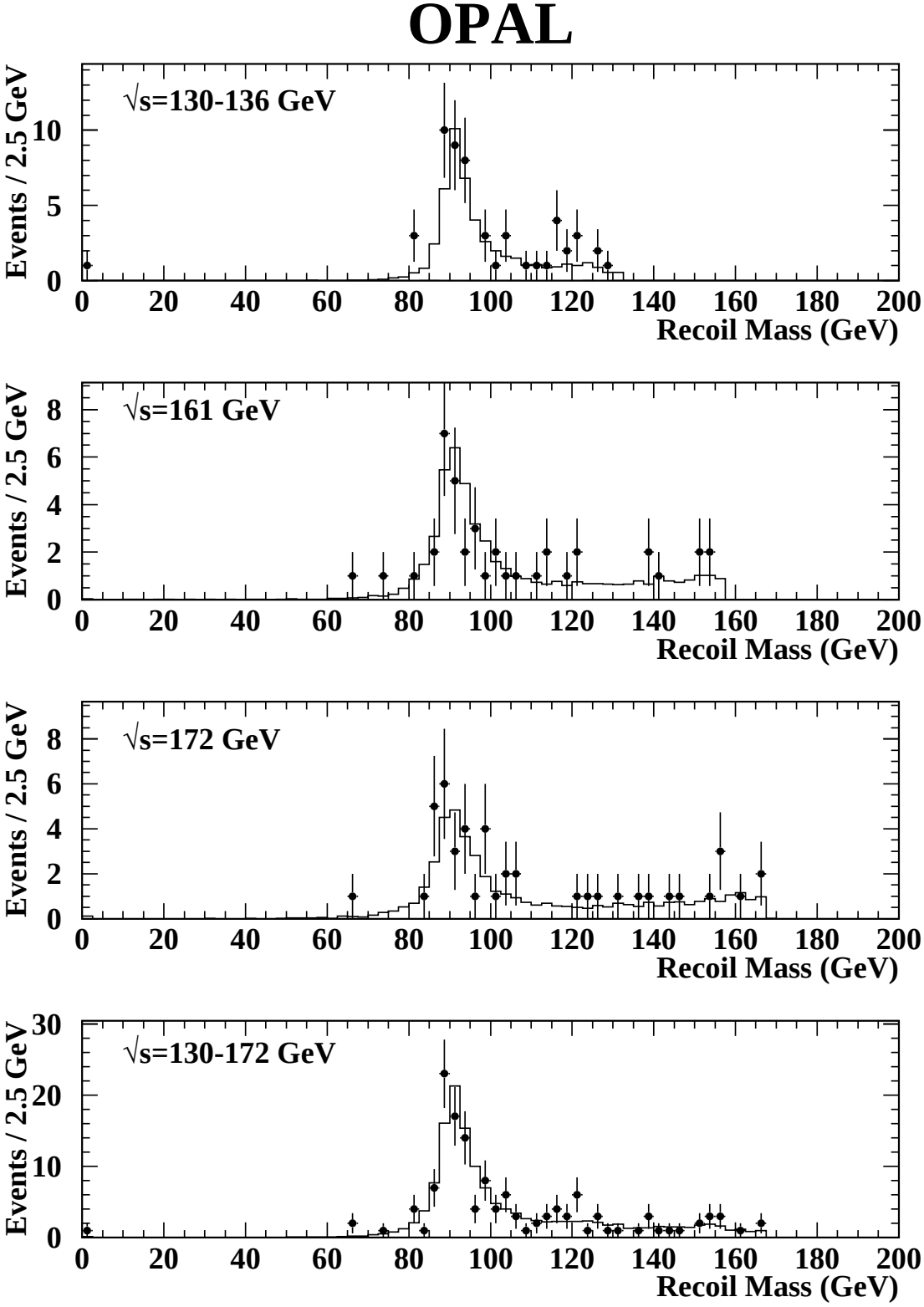

Figure 4: The recoil mass distribution for events passing the single photon selection for the $\sqrt{s}$ = 130-136 GeV, 161 GeV, 172 GeV, and combined 130 - 172 GeV data samples. The points with error bars are the data and the histograms are the expectations from the KORALZ $e^+e^- \to \nu\overline{\nu}\gamma(\gamma)$ Monte Carlo normalized to the integrated luminosity of the data.

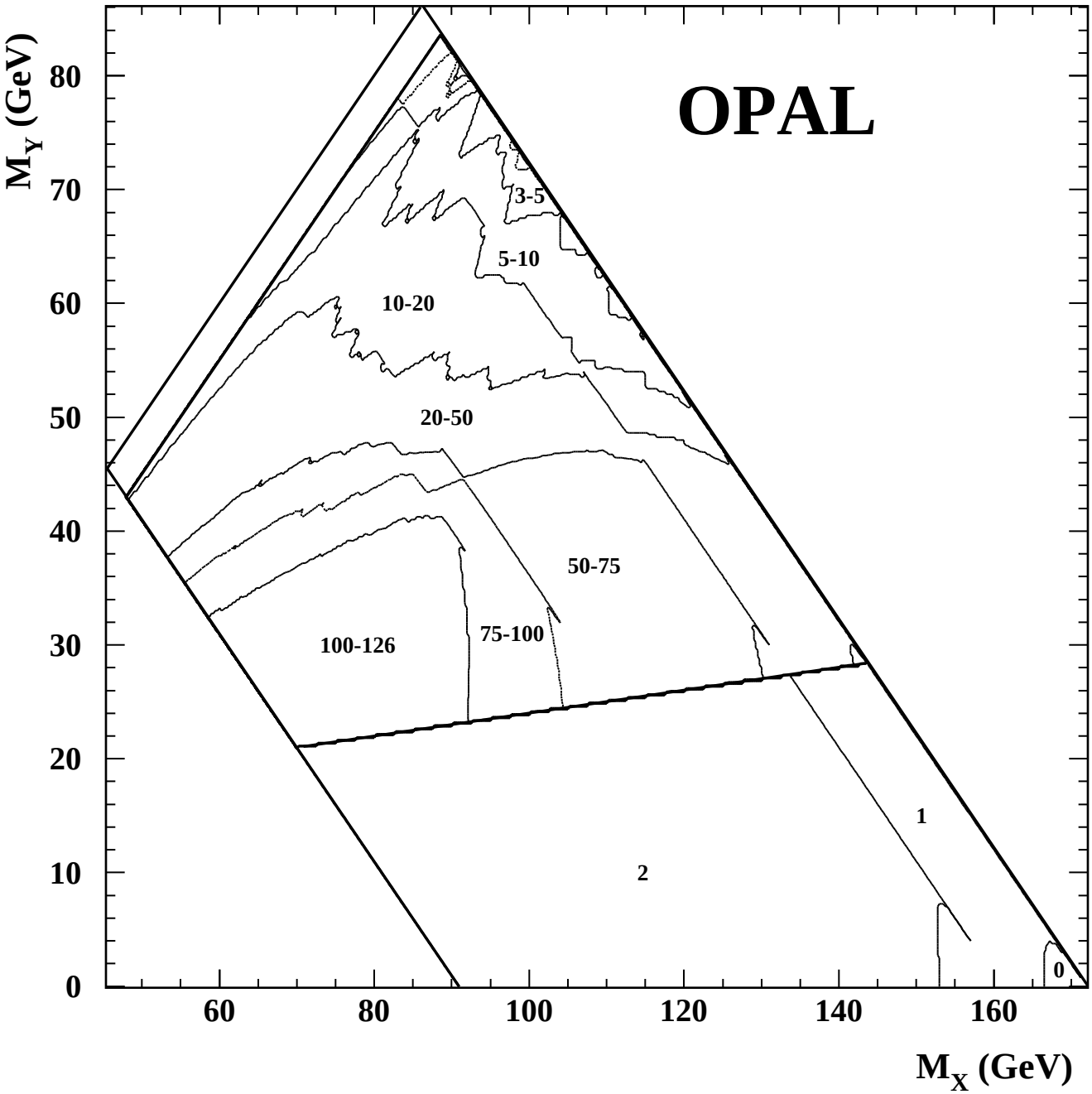

Figure 5: Number of single photon candidate events in the combined data sample ($\sqrt{s}$ = 130-172 GeV) consistent with each set of mass values ($M_{\rm X}$, $M_{\rm Y}$) for the process $e^+e^- \to {\rm XY}$, ${\rm X} \to {\rm Y}\gamma$, after application of all selection criteria including kinematic consistency requirements. Lines are drawn around the boundaries defined by $M_{\rm X} + M_{\rm Y} = 172$ GeV, $M_{\rm X} = M_{\rm Y}$, and $M_{\rm X} + M_{\rm Y} = M_{\rm Z}$, and to display the boundary between the small and large $M_{\rm Y}$ regions. Regions defined by $M_{\rm X} - M_{\rm Y} < 5$ GeV and $M_{\rm X} + M_{\rm Y} < M_{\rm Z}$ are not considered in limit calculations, and no events are displayed in these regions.

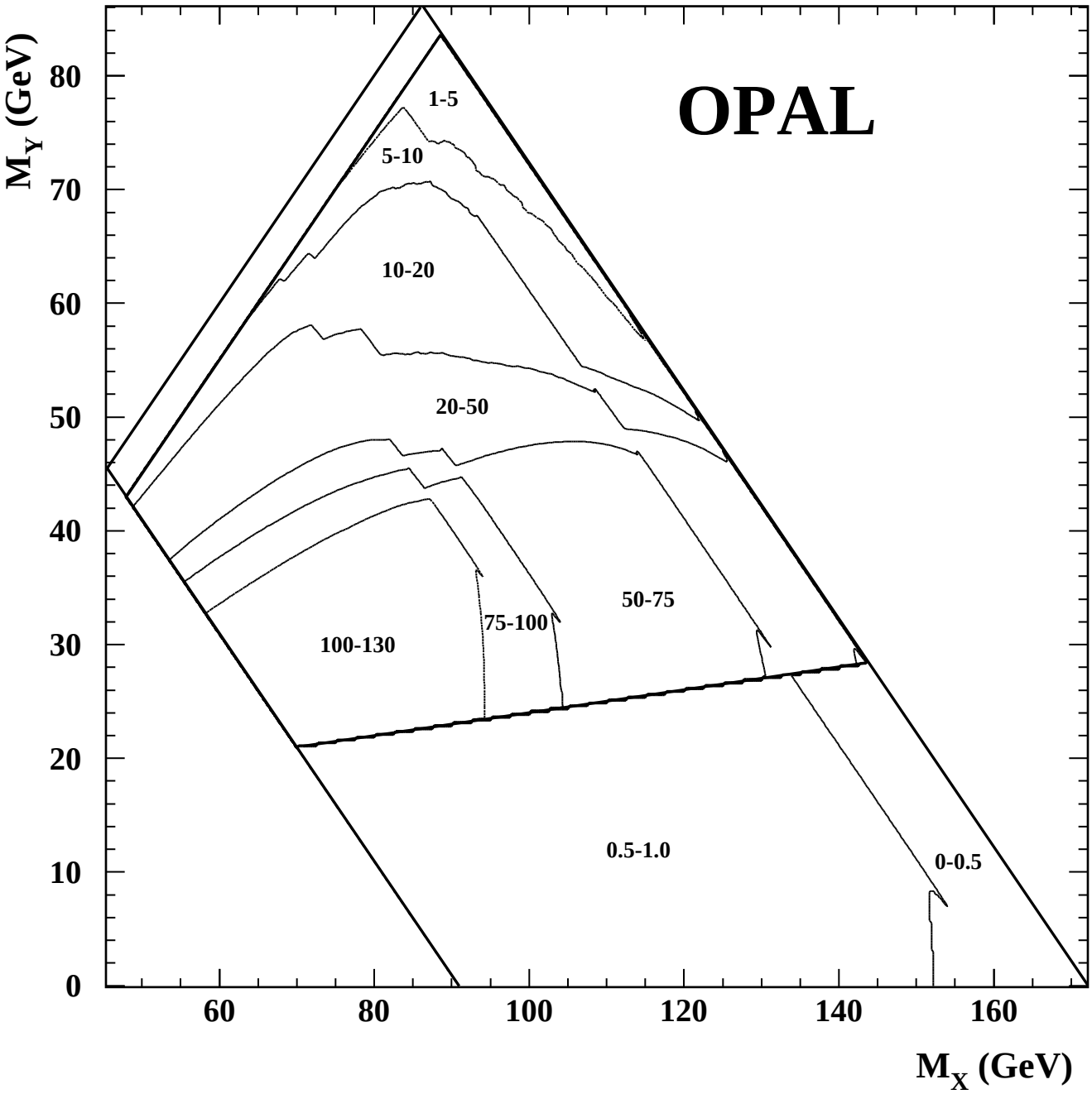

Figure 6: Number of Standard Model $\nu\bar{\nu}\gamma(\gamma)$ events predicted by KORALZ to pass all single photon selection criteria for the combined data sample ($\sqrt{s}$ = 130-172 GeV), which are consistent with the process $e^+e^- \to XY$, $X \to Y\gamma$ at each set of mass values (M_X, M_Y). This figure gives the expected Standard Model contribution to Figure 5. Boundaries and delineated regions are the same as in Figure 5.

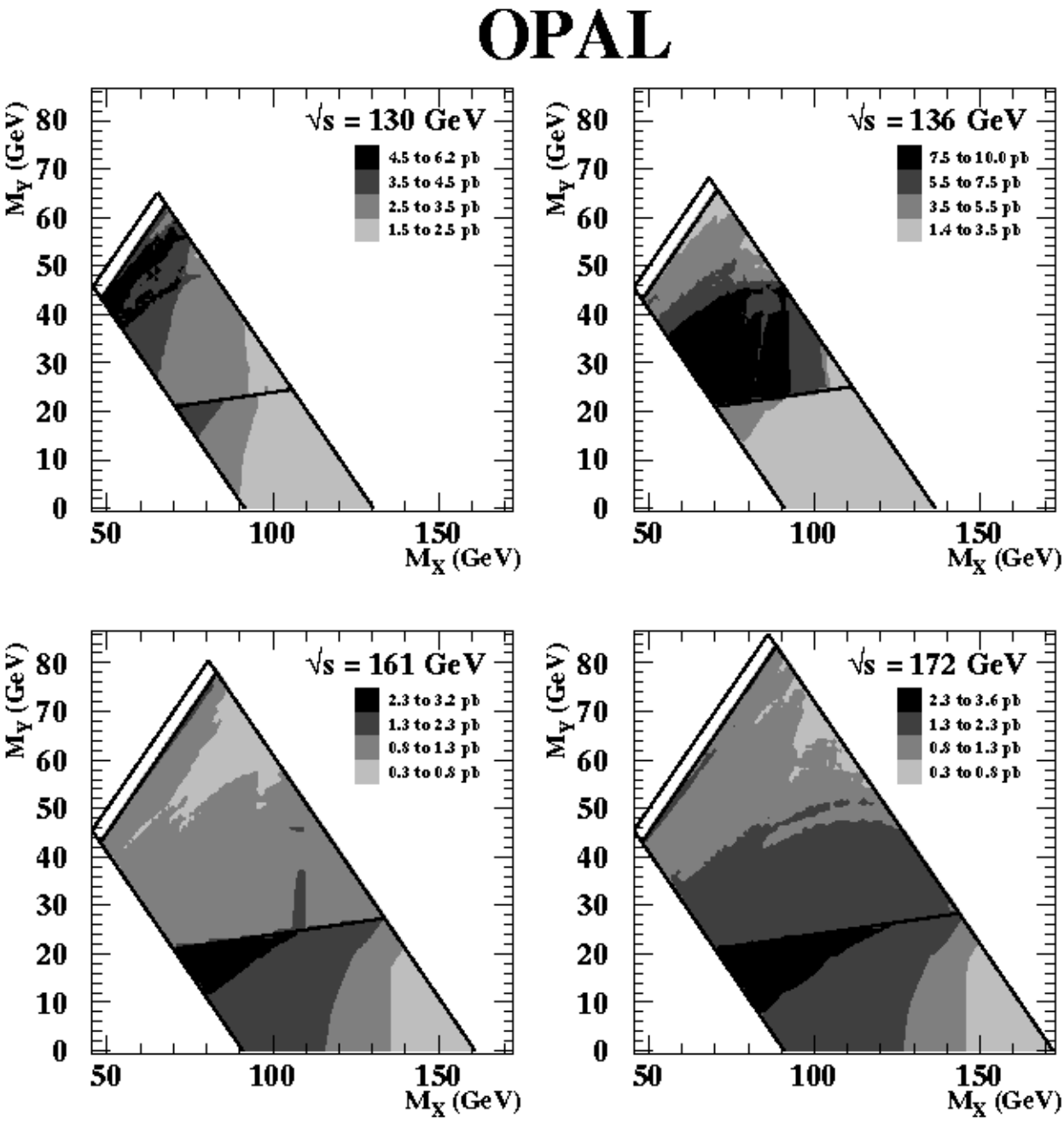

Figure 7: 95% CL upper limits on $\sigma(\mathrm{e^+e^-} \to \mathrm{XY}) \cdot \mathrm{BR}(\mathrm{X} \to \mathrm{Y}\gamma)$ as a function of M_X and M_Y at each centre-of-mass energy. Lines are drawn to indicate the kinematically allowed boundaries defined by $M_\mathrm{X} + M_\mathrm{Y} = \sqrt{s}$. Other boundaries and delineated regions are as defined for Figure 5.

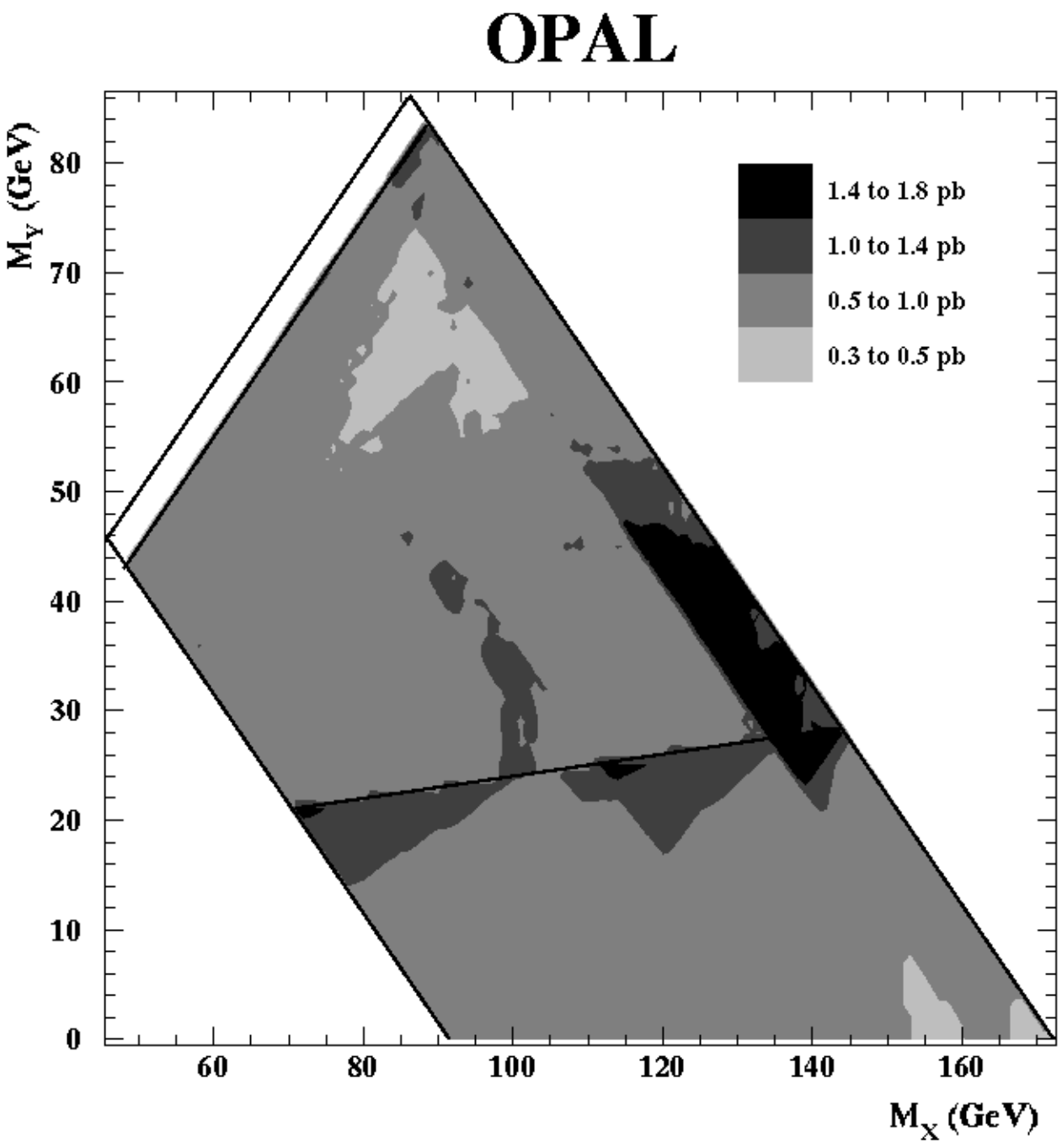

Figure 8: The 95% CL upper limit on $\sigma(\mathrm{e^+e^-} \to \mathrm{XY}) \cdot \mathrm{BR}(\mathrm{X} \to \mathrm{Y}\gamma)$ at $\sqrt{s} = 172$ GeV as a function of M_X and M_Y, obtained from the combined data sample assuming a cross-section scaling of β_X/s. The boundaries and delineated regions are as defined for Figure 5.

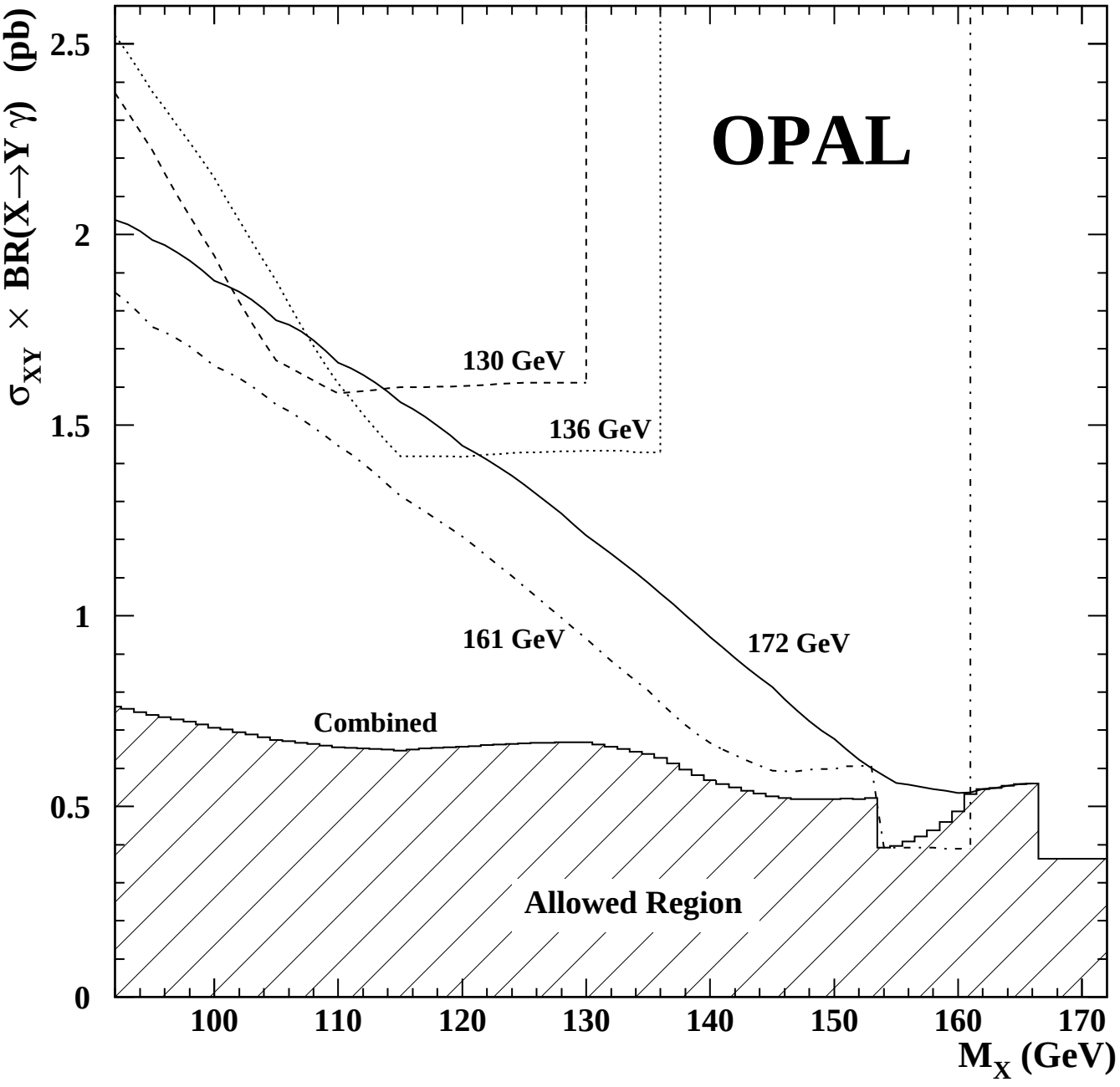

Figure 9: The 95% CL upper limits on $\sigma(\mathrm{e^+e^-} \to \mathrm{XY}) \cdot \mathrm{BR}(\mathrm{X} \to \mathrm{Y}\gamma)$ as a function of M_X, assuming $M_\mathrm{Y} \approx 0$, for each centre-of-mass energy. The upper limit on $\sigma(\mathrm{e^+e^-} \to \mathrm{XY}) \cdot \mathrm{BR}(\mathrm{X} \to \mathrm{Y}\gamma)$, evaluated at $\sqrt{s} = 172$ GeV, obtained from the combined data sample is also shown. The combination was performed assuming a cross-section scaling of β_X/s. The allowed region is shaded.

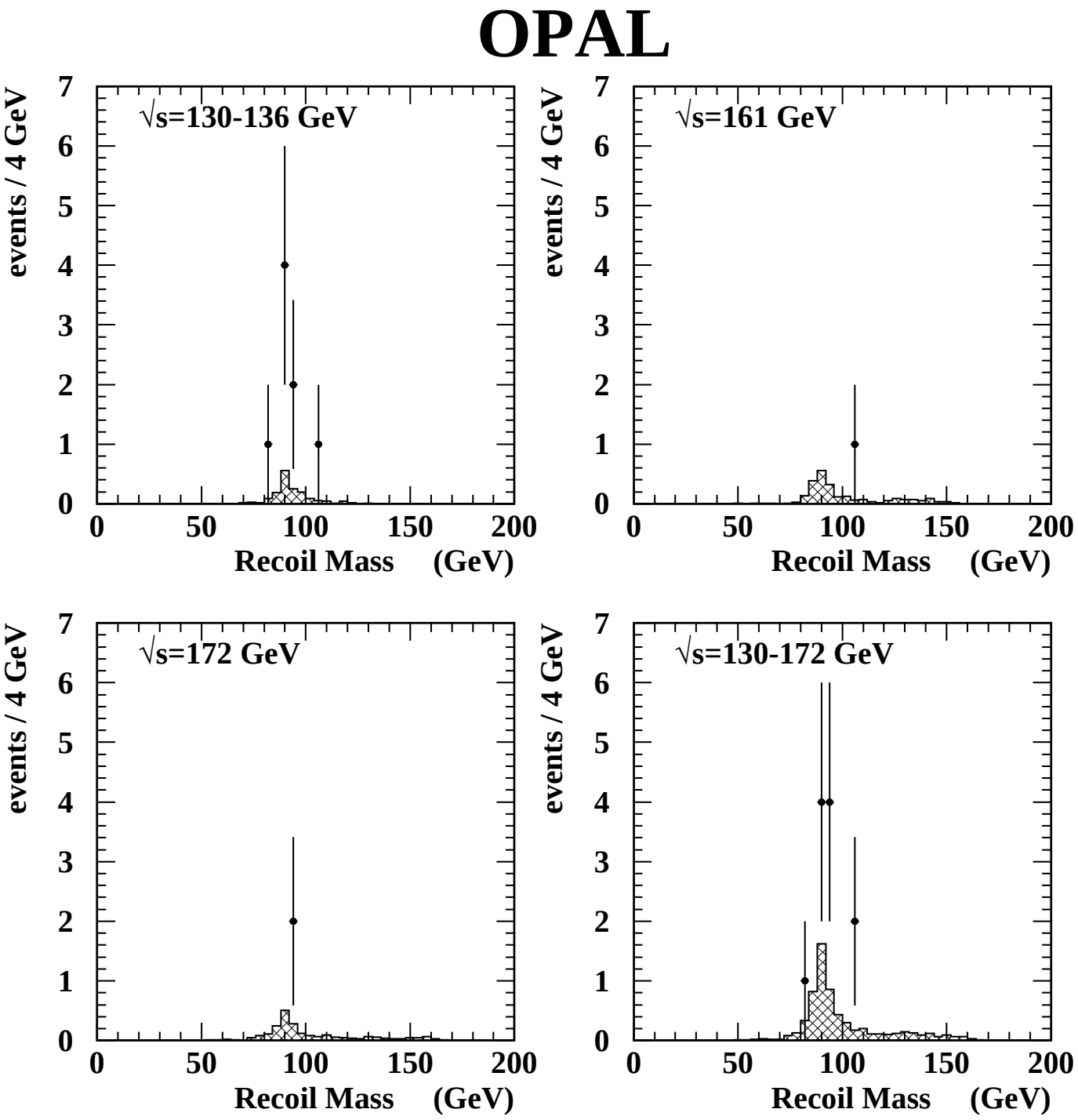

Figure 10: Recoil-mass distributions for the selected acoplanar-photons events for each centre-of-mass region and for the combined data sample. The data points with error bars represent the selected OPAL data events. In each case the shaded histogram shows the expected contribution from $e^+e^- \to \nu\overline{\nu}\gamma\gamma(\gamma)$ events, normalized to the total integrated luminosity. The KORALZ generator was used for these distributions.

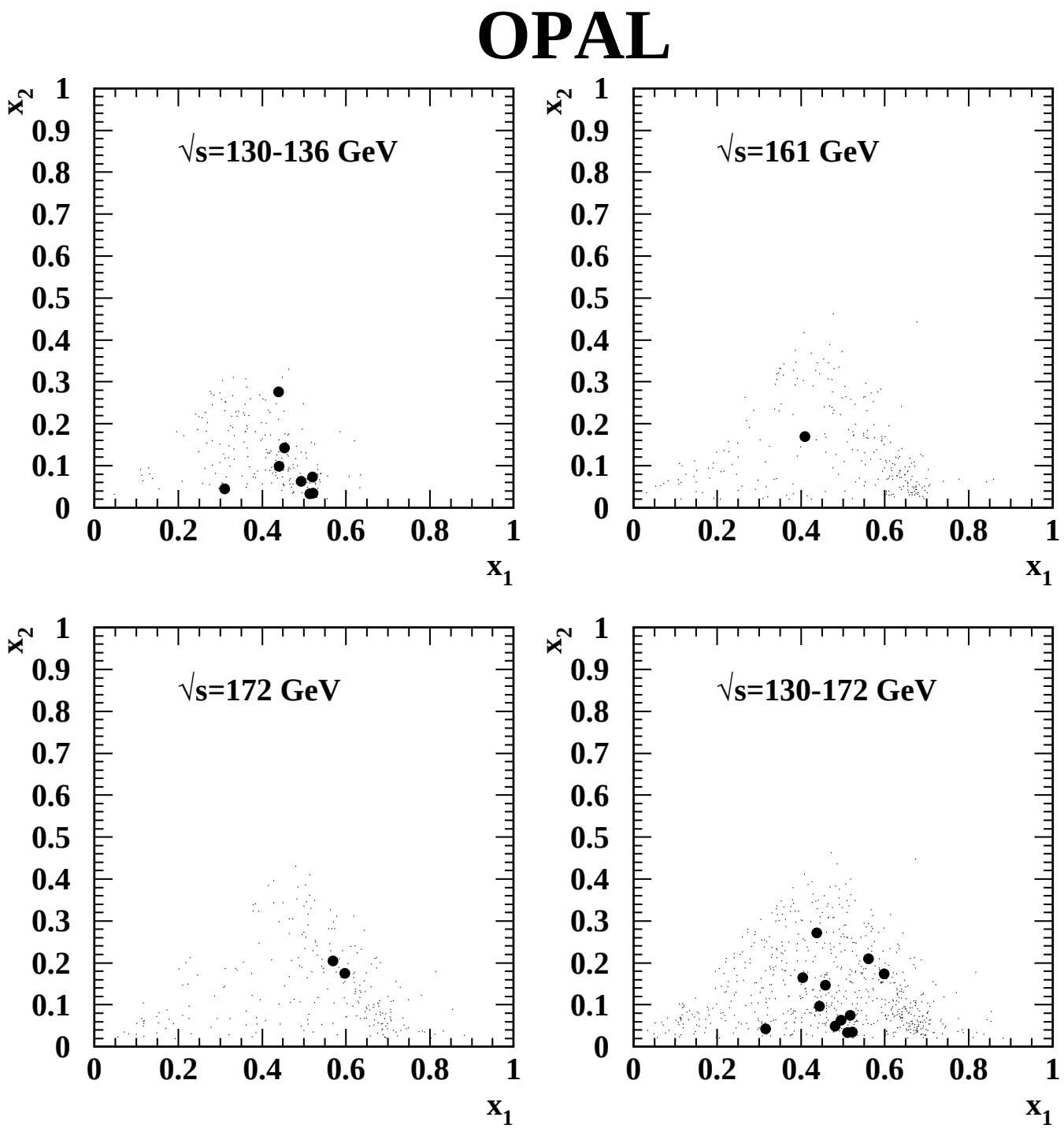

Figure 11: x_2 vs x_1 for the selected acoplanar-photons events for each centre-of-mass region and for the combined data sample. The large points represent the selected OPAL data events. The smaller dots show the expected distribution for events from the process $e^+e^- \to \nu\overline{\nu}\gamma\gamma(\gamma)$ events, from KORALZ. The normalization of the Monte Carlo distributions is arbitrary. However, for the combined plot the relative normalizations of the various data samples is maintained.

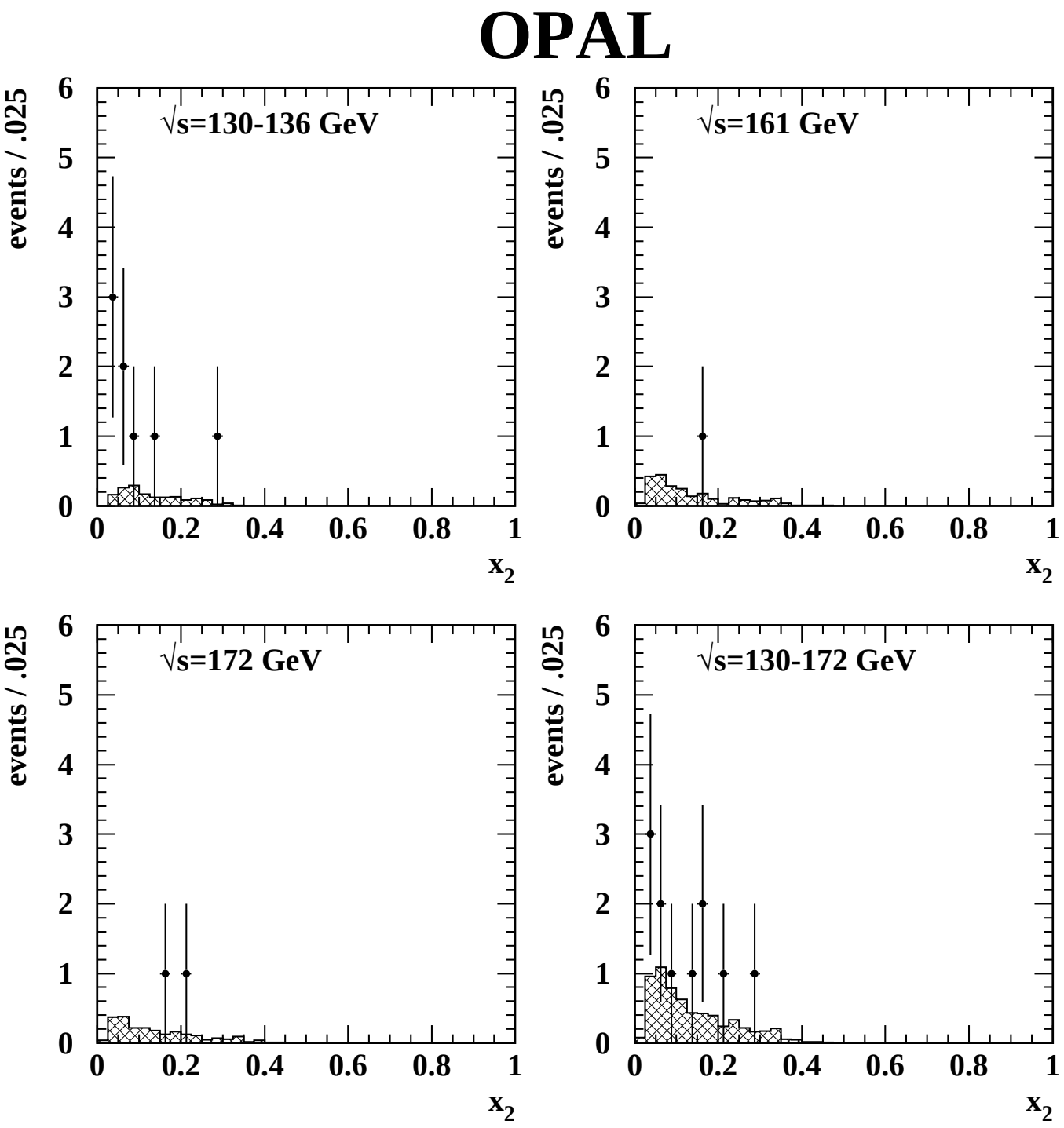

Figure 12: Distributions of scaled energy of the lower energy photon for the selected acoplanar-photons events for each centre-of-mass region and for the combined data sample. The data points with error bars represent the selected OPAL data events. In each case the shaded histogram shows the expected contribution from $e^+e^- \to \nu\overline{\nu}\gamma\gamma(\gamma)$ events, normalized to the total integrated luminosity. The KORALZ generator was used for these distributions.

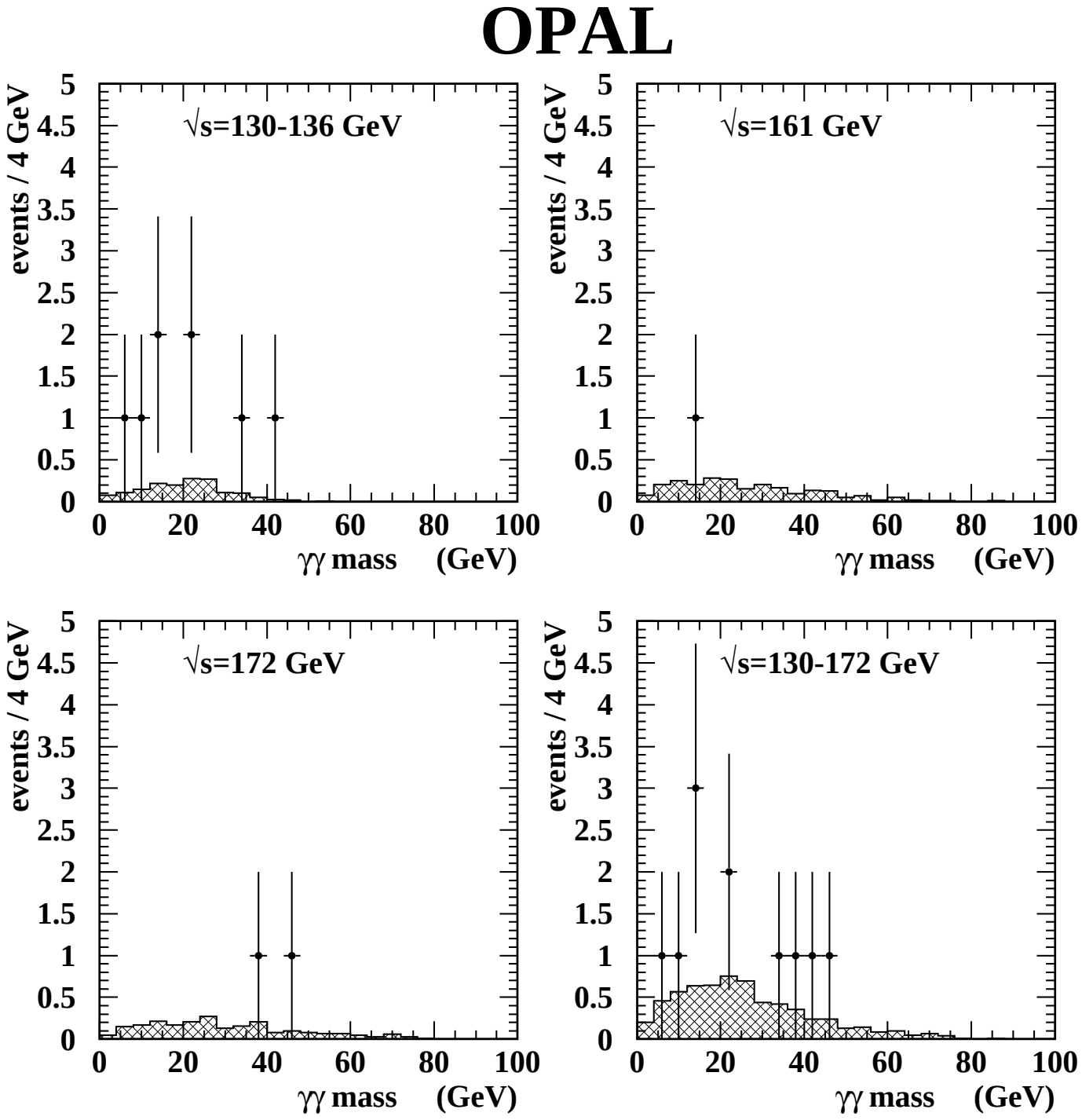

Figure 13: Distributions of the $\gamma\gamma$ invariant mass of the accepted acoplanar-photon pairs for each centre-of-mass region. The points with error bars represent the OPAL data while the shaded histograms show the predicted distributions for events from $e^+e^- \to \nu\overline{\nu}\gamma\gamma(\gamma)$ events, from KORALZ, normalized to the corresponding integrated luminosity.

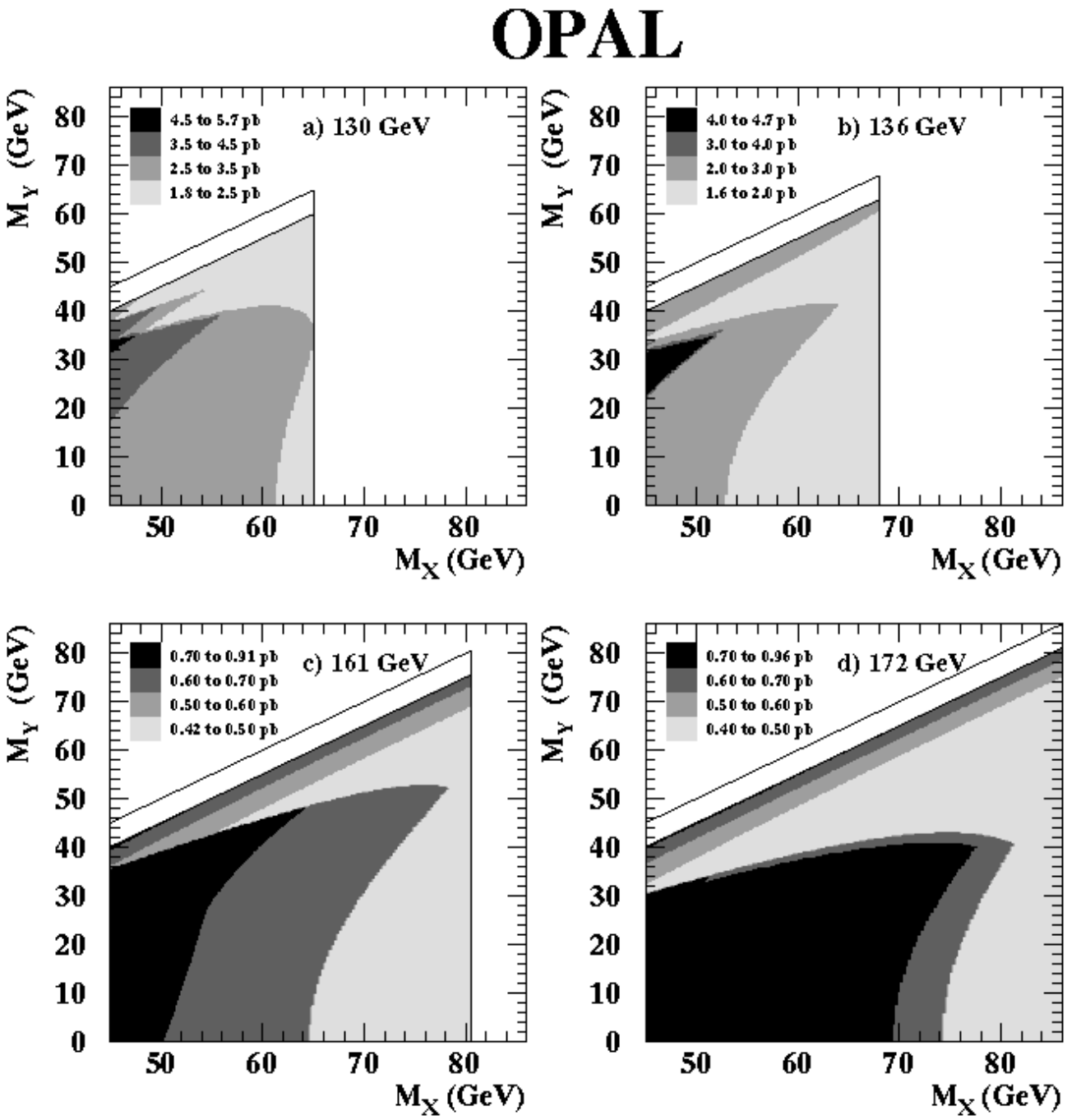

Figure 14: For each centre-of-mass energy, the shaded areas show 95% CL exclusion regions for $\sigma(\mathrm{e^+e^-} \to \mathrm{XX}) \cdot \mathrm{BR}^2(\mathrm{X} \to \mathrm{Y}\gamma)$. No limit is set for mass-difference values $M_\mathrm{X} - M_\mathrm{Y} < 5$ GeV, defined by the lower line above the shaded regions. The upper line is for $M_\mathrm{X} = M_\mathrm{Y}$.

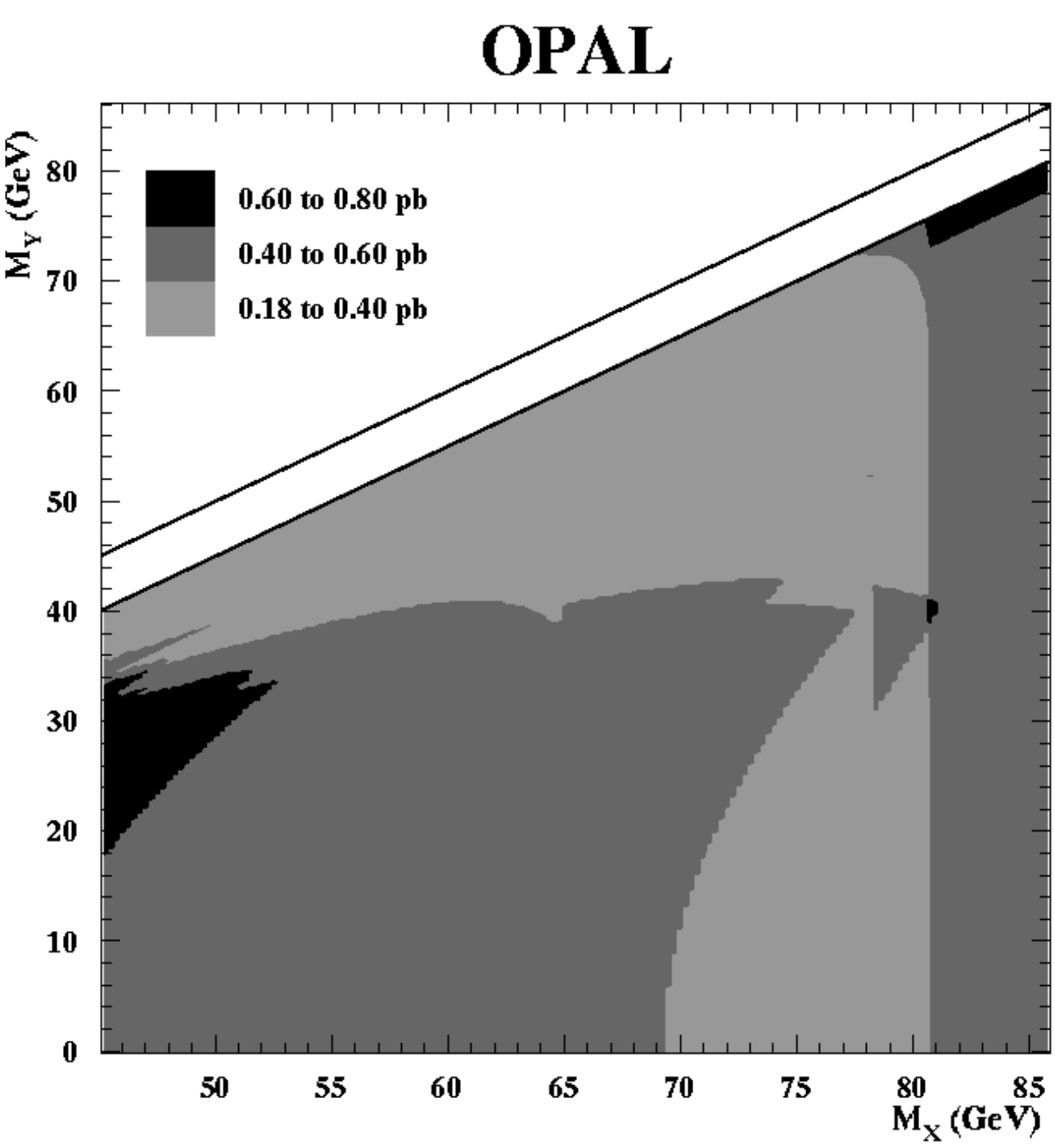

Figure 15: The shaded areas show 95% CL exclusion regions for $\sigma(e^+e^- \to XX) \cdot BR^2(X \to Y\gamma)$ at $\sqrt{s} = 172$ GeV, obtained from the combined data sample assuming a cross-section scaling of β_X/s. No limit is set for mass-difference values $M_X - M_Y < 5$, defined by the lower line above the shaded regions. The upper line is for $M_X = M_Y$.

cp

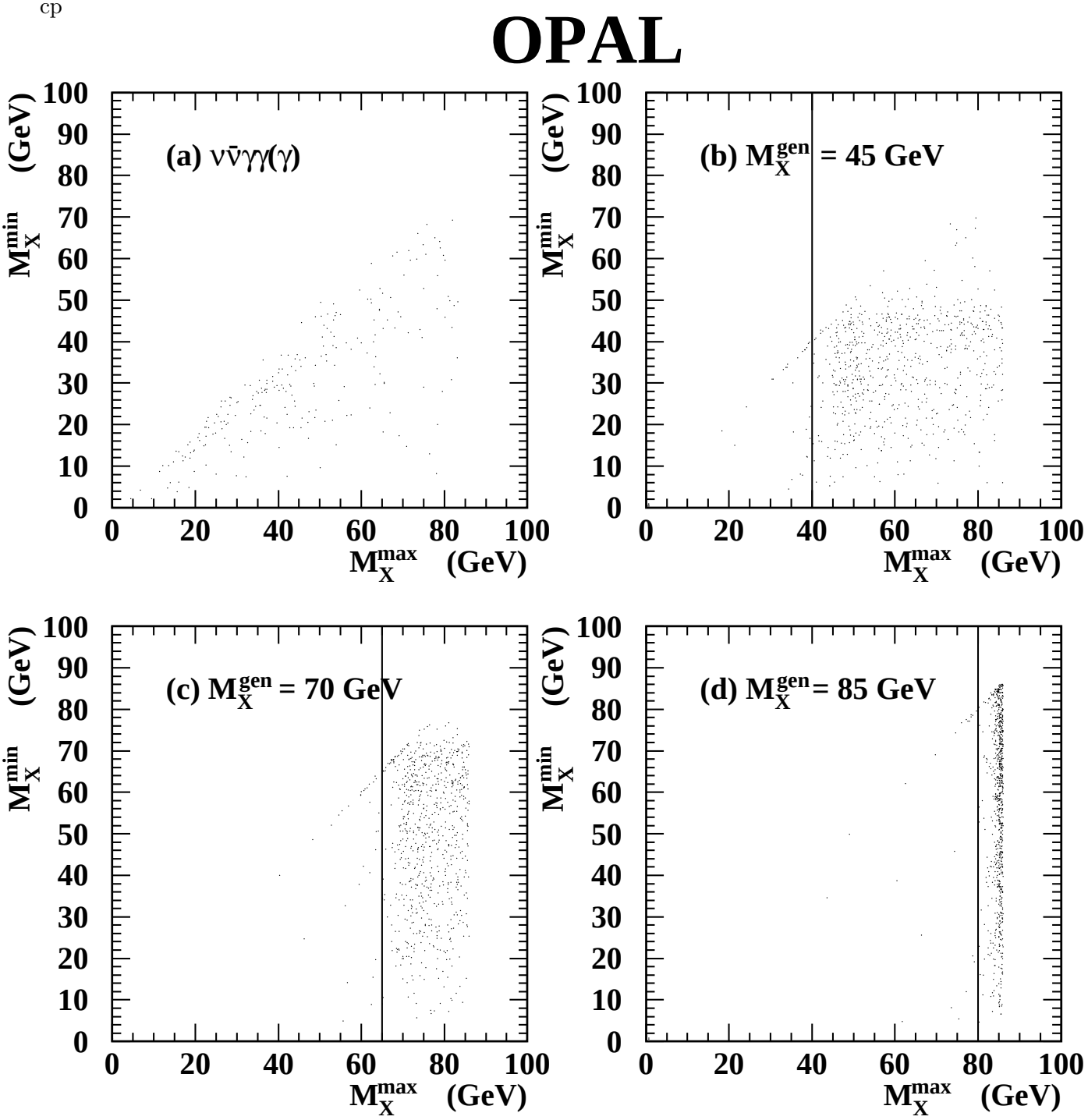

Figure 16: $M_{\mathrm{X}}^{\mathrm{min}}$ vs. $M_{\mathrm{X}}^{\mathrm{max}}$ for (a) $\nu\overline{\nu}\gamma\gamma(\gamma)$ Monte Carlo (KORALZ) and (b)-(d) $\mathrm{e^+e^-} \rightarrow \mathrm{XX}$, $\mathrm{X} \rightarrow \mathrm{Y}\gamma$, $M_{\mathrm{Y}} \approx 0$ Monte Carlo (SUSYGEN) for various M_{X}. The vertical lines represent the chosen cut values discussed in the text. These are for Monte Carlo generated at a centre-of-mass energy of 172 GeV.

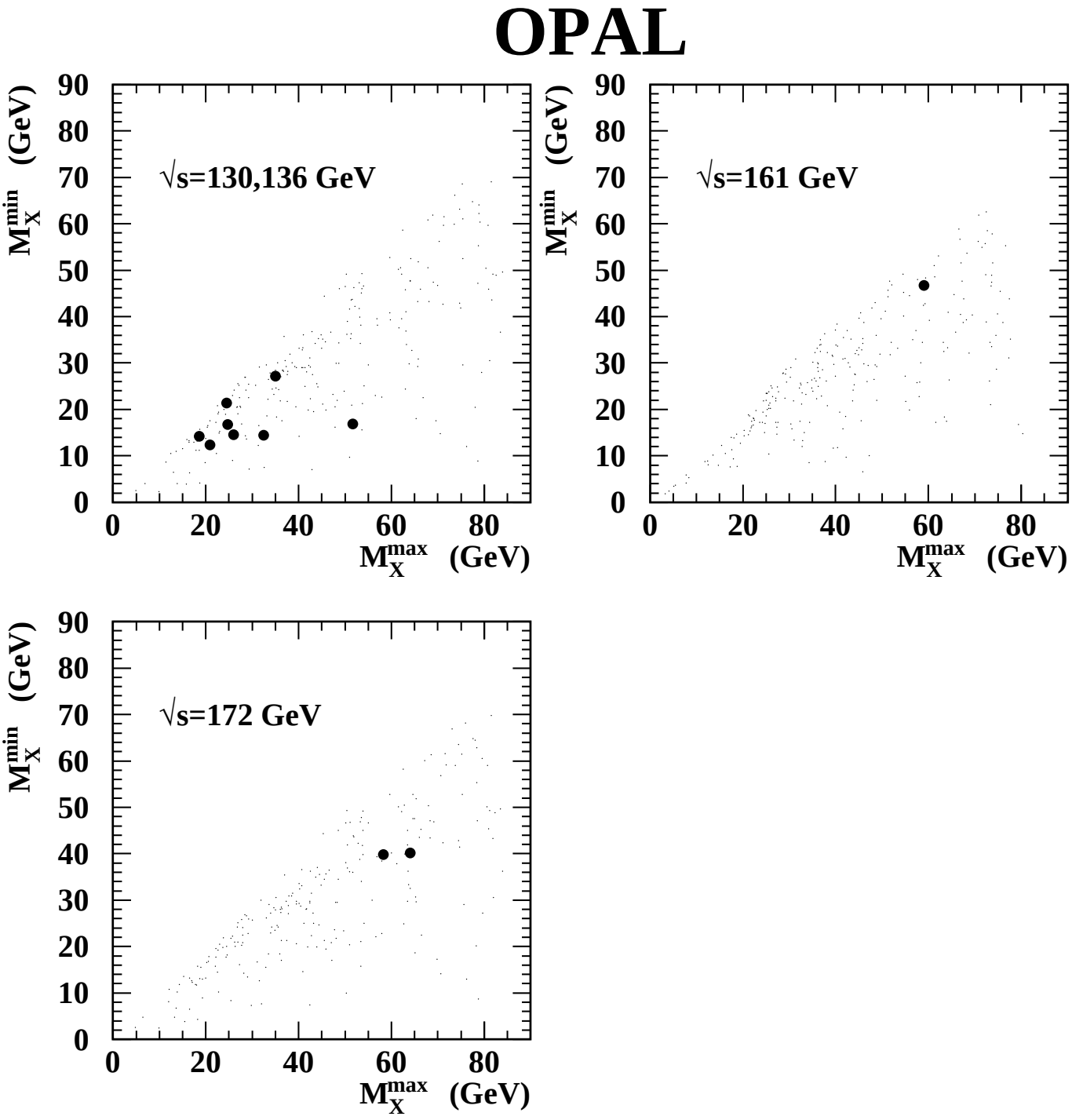

Figure 17: $M_{\mathrm{X}}^{\mathrm{min}}$ vs. $M_{\mathrm{X}}^{\mathrm{max}}$ for the accepted acoplanar-photons events for each centre-of-mass energy region. Overlaid are the expected distributions for contributions from the Standard Model process $\mathrm{e^+e^-} \to \nu\overline{\nu}\gamma\gamma(\gamma)$, from the KORALZ generator.

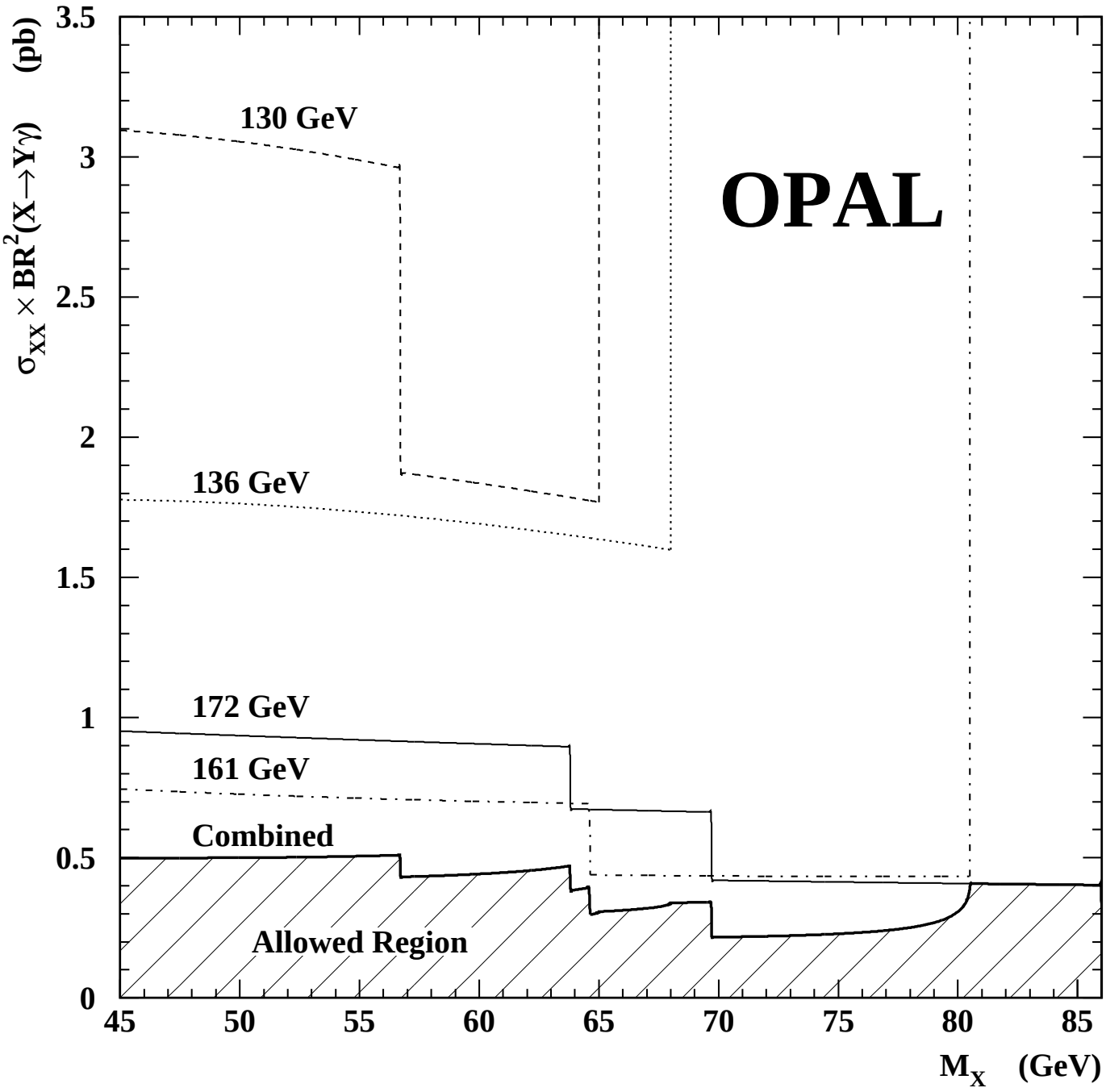

Figure 18: The 95% confidence level upper limit on $\sigma(e^+e^- \to XX) \cdot BR^2(X \to Y\gamma)$ for the case $M_Y \approx 0$, as a function of M_X, for each value of $\sqrt{s}$. Also shown is the limit, evaluated at $\sqrt{s} = 172$ GeV, obtained from the combined data sample assuming a cross-section scaling of β_X/s.

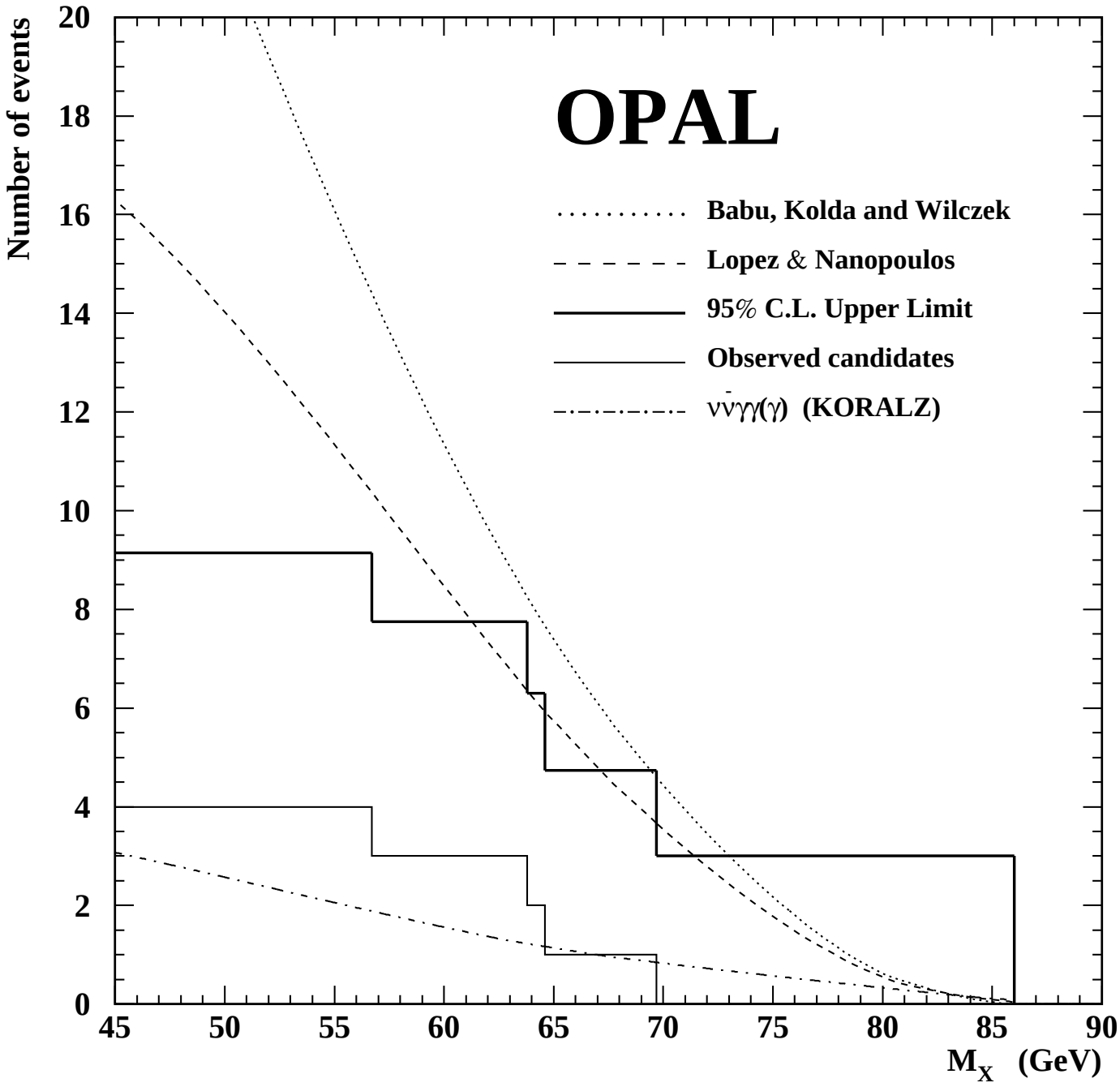

Figure 19: Results for $e^+e^- \to XX$, $X \to Y\gamma$, with $M_Y \approx 0$ for the combined data sample. The lower solid line shows the number of observed candidates consistent with a given value of M_X. The dashed-dotted line shows the expected contribution from $\nu\overline{\nu}\gamma\gamma(\gamma)$ obtained from the KORALZ generator. The thick solid line shows the 95% confidence level upper limit on the number of candidate events. The dashed (dotted) line shows the expected number of events from the model of Lopez and Nanopoulos [14] (Babu, Kolda and Wilczek [16]). Within these models, $\tilde{\chi}_1^0$ masses less than 61.3 (69.4) GeV are excluded at the 95% confidence level.